4-19-2021

A high-androgen microenvironment inhibits granulosa cell proliferation and alters cell identity

Renee McFee Fee
University of Nebraska-Lincoln, rmcfee3@unl.edu

Sarah Romereim
University of Nebraska-Lincoln, sromereim2@unl.edu

Alexandria P. Snider
University of Nebraska-Lincoln, alex.snider@unl.edu

Adam F. Summers
New Mexico State University, adamfsummers@gmail.com

William E. Pohlmeier
University of Nebraska-Lincoln, wpohlmeier2@unl.edu

See next page for additional authors

Molecular and Cellular Endocrinology 531 (2021) 111288

Contents lists available at ScienceDirect

Molecular and Cellular Endocrinology

journal homepage: www.elsevier.com/locate/mce

A high-androgen microenvironment inhibits granulosa cell proliferation and alters cell identity

Renee M. McFee [a,1], Sarah M. Romereim [b,1,2], Alexandria P. Snider [b,3], Adam F. Summers, PhD [c], William E. Pohlmeier [b], Scott G. Kurz [b], Robert A. Cushman [d], John S. Davis [e,f], Jennifer R. Wood [b], Andrea S. Cupp [b,*]

[a] University of Nebraska-Lincoln, School of Veterinary Medicine and Biomedical Sciences, P.O. Box 830905, Lincoln, NE, 68583-0905, USA
[b] University of Nebraska–Lincoln, Department of Animal Science, 3940 Fair Street, Lincoln, NE, 68583-0908, USA
[c] New Mexico State University, Animal and Range Sciences, Knox Hall Room 202, MSC 3-I Las Cruces, NM 88003, USA
[d] USDA, Agricultural Research Service, U.S. Meat Animal Research Center, P.O. Box 166, Clay Center, NE, 68933, USA
[e] University of Nebraska Medical Center, Olson Center for Women's Health, 983255 Nebraska Medical Center, Omaha, NE, 68198-3255, USA
[f] VA Nebraska-Western Iowa Health Care System, Omaha, NE, 68105, USA

ARTICLE INFO

Keywords:
Bovine granulosa
Excess androgens
Transcriptome
Cell cycle arrest
Cell identity
AMH

ABSTRACT

A naturally occurring bovine model with excess follicular fluid androstenedione (High A4), reduced fertility, and polycystic ovary syndrome (PCOS)-like characteristics has been identified. We hypothesized High A4 granulosa cells (GCs) would exhibit altered cell proliferation and/or steroidogenesis. Microarrays of Control and High A4 GCs combined with Ingenuity Pathway Analysis indicated that High A4 GCs had cell cycle inhibition and increased expression of microRNAs that inhibit cell cycle genes. Granulosa cell culture confirmed that A4 treatment decreased GC proliferation, increased anti-Müllerian hormone, and increased mRNA for *CTNNBIP1*. Increased *CTNNBIP1* prevents CTNNB1 from interacting with members of the WNT signaling pathway thereby inhibiting the cell cycle. Expression of CYP17A1 was upregulated in High A4 GCs presumably due to reduced FOS mRNA expression compared to Control granulosa cells. Furthermore, comparisons of High A4 GC with thecal and luteal cell transcriptomes indicated an altered cellular identity and function contributing to a PCOS-like phenotype.

1. Introduction

It is well established that high androgen concentrations, both circulating and within the ovary, are associated with ovarian dysfunction and systemic metabolic issues. Ovarian hyperandrogenism as seen with polycystic ovary syndrome (PCOS) causes symptoms such as hirsutism, anovulation, and metabolic dysfunction (which also compounds fertility problems) (Azziz et al., 2009; Hayek et al., 2016; Padwal, 2020; Rosenfield and Ehrmann, 2016). Other causes of hyperandrogenism such as congenital adrenal hyperplasia also result in reproductive disruptions (e.g. precocious puberty), virilization, and metabolic syndromes (Azziz et al., 2004; Hayek et al., 2016; Merke and Bornstein, 2005; Rosenfield and Ehrmann, 2016). Androgens affect many systems, including the hypothalamic-pituitary-gonadal axis. Disrupted regulation of gonadotropin releasing hormone and gonadotropins are sufficient to substantially impact fertility (Bateman and Patisaul, 2008; Dierich et al., 1998; Viau, 2002). There are also local effects of androgens on the follicular cells within the ovary. The theca cells of the follicle are

Abbreviations: A4, androstenedione; GCs, granulosa cells; IPA, Ingenuity Pathway Analysis; LLCs, large luteal cells; PCA, Principal Component Analysis; PCOS, Polycystic Ovary Syndrome; SLCs, small luteal cells; TCs, theca cells; AMH, Anti-Mullerian Hormone; CTNNB1, beta-catenin; CTNNBIP1, catenin beta interacting protein 1; WNT, wingless-type mouse mammary tumor virus integration site.

* Corresponding author. Department of Animal Science, University of Nebraska-Lincoln, USA.
E-mail address: acupp2@unl.edu (A.S. Cupp).
[1] Both authors contributed equally to this manuscript- Co-first authors.
[2] Present address: Musculoskeletal Institute, Orthopedic Biology Research, Atrium Health, 1000 Blythe Blvd., Charlotte, NC, 28203, USA, sarah.romereim@atriumhealth.org.
[3] Present address: USDA, ARS, U.S. Meat Animal Research Center, Livestock Biosystems Research Unit, Clay Center, Nebraska 68933, Alex.Snider@usda.gov.

https://doi.org/10.1016/j.mce.2021.111288
Received 31 December 2020; Received in revised form 17 April 2021; Accepted 19 April 2021
Available online 24 April 2021

primarily responsible for converting cholesterol to androgens, while the granulosa cells (GCs) convert thecal androgens to estrogens (Mason et al., 1994; Young and McNeilly, 2010). However, bovine GCs also express enzymes that can convert 17-hydroxy-pregnenolone to the androgens dehydroepiandrosterone (DHEA) and androstenedione (A4) in a steroid synthesis pathway that is shared between humans and cattle (Conley et al., 1995; Conley and Bird, 1997). Human and bovine GCs also express the androgen receptor and can thus respond to local androgens as well as produce them (Hampton et al., 2004; Luo and Wiltbank, 2006).

It can be difficult to isolate local ovarian versus systemic effects on fertility in most clinical cases of hyperandrogenism because there is a broad spectrum of symptoms (Azziz et al., 2004; Balen et al., 1995). Many cases of infertility can occur without excessive circulating androgens (Hayek et al., 2016; Padwal, 2020; Rosenfield and Ehrmann, 2016) and mild cases of sporadic anovulation can go undetected. Examination of a cohort of normally menstruating women demonstrated that 8–13% of these 'normal' women were not consistently ovulating for two consecutive reproductive cycles (Hambridge et al., 2013; Lynch et al., 2014). While infertility and sporadic anovulation can have a plethora of causes, high local concentrations of androgens not accompanied by high circulating concentrations of androgens may be a contributing factor to these disorders.

Cattle are a monovulatory species with similar reproductive cycles to those of women making them an excellent research model for ovarian physiology. In fact, beef cows have many similar ovarian problems (Abedaj-Majed and Cupp, 2019). These issues include the spontaneous development of ovarian cysts and chronic or sporadic anovulation in approximately 10% of females (Smith, 2015; Summers et al., 2014; Wiltbank et al., 2002). A population of beef cows within the University of Nebraska-Lincoln research herd has been identified with both a theca cell molecular phenotype similar to that seen in women with PCOS and excessive intrafollicular A4, the predominant androgen in cattle (Summers et al., 2014). These cows exhibit excess concentrations of A4 in their follicular fluid (>30 fold higher than controls). Additionally, these cows lack an increase in estradiol (E2) production of similar magnitude to the follicular A4 concentrations (only 2–4 fold higher) (Summers et al., 2014).

The identification of this phenotype presents a novel opportunity to identify the local ovarian effects of naturally-occurring androgen excess *in vivo*. The primary cause of the increased A4 was identified as excessive steroidogenesis in the theca cells of the dominant follicle (Summers et al., 2014). The effects of those androgens and how they can lead to anovulation have been further investigated by assessing the consequences for the GCs of those same dominant follicles.

2. Methods

2.1. 1a. Ethics statement

All animals were humanely treated and cared for in accordance with University of Nebraska-Lincoln IACUC guidelines. The University of Nebraska-Lincoln is fully AAALAC accredited and follows NIH guidelines. Transcriptomes of granulosa cells were evaluated in this study. Only females were used in the current study since we are interested in the mechanisms involved with granulosa cell function, which is only present in female mammalian species.

2.2. 1b. Cow classification

A multi-year, multiple estrous cycle survey of 26 randomly selected cows was performed to characterize reproductive phenotypes in the University of Nebraska-Lincoln physiology herd located at the Eastern Nebraska Research and Extension Center (ENREC) formerly known as the Agriculture Research and Development Center (ARDC) (Summers et al., 2014). The estrous cycles of these beef cows (75% Red Angus, 25% MARC III) were synchronized with two injections of prostaglandinF2α (PGF2α) 14 days apart and transrectal ultrasound-guided ovarian follicle aspiration was performed 12–36 h after the final PGF2α injection as previously described (Summers et al., 2014) and Fig. 1.

The synchronization protocol in Fig. 1 is the most "natural" synchronization method that does not introduce steroids into the cow to alter development of the dominant follicle. Instead, it uses a normally expressed factor PGF2α to lyse the corpus luteum causing the most advanced follicle to initiate growth and development to an ovulatory stage follicle which can be aspirated 12–36 h later and A4 measured in ff.

Follicles aspirated 12–36 time points after PGF2α would not be expected to have been exposed to a luteinizing hormone (LH) surge. Previous experiments in our cattle have shown that the LH surge occurs 56–72 h after PGF2α administration (data not shown) while others have shown that the LH surge occurs > 42 h post-PGF2α (Guilbault et al., 1988; Nkuuhe and Manns 1985). The follicular fluid of the dominant follicle was aspirated and separated from GCs by centrifugation. Subsequent radioimmunoassay for E2 and enzyme-linked immunosorbent assay (ELISA) for A4 were performed as previously described (Summers et al., 2014). Based on these assays, follicles with a high A4 concentration ([A4] ≥40 ng/mL) and no corresponding increase in [E2] were classified as "High A4", while follicles with an average/Control concentration (A4 ≤20 ng/mL) and average [E2] were classified as "Low A4" and designated as Controls.

2.3. Ovariectomy, follicle aspiration and isolation of somatic cells from Control and High A4 cows for microarray analysis

Ovariectomy was performed approximately 36 h after CIDR removal (Youngquist et al., 1995). Upon ovariectomy, one follicle, the dominant, largest (>10 mm diameter) antral follicle from each cow's ovaries was aspirated/dissected and the GCs (≥94% purity; Romereim et al., 2017) and follicular fluid were isolated as previously described (Summers et al., 2014). Follicles with a follicular fluid E2:P4 ratio greater than 1 were classified as estrogen-active (EA; Echternkamp et al., 2004; Sunderland et al., 1994). After checking that the largest follicle was EA, the granulosa cells were then used for the microarray and subsequent quantitative real-time PCR (qPCR), GCs were homogenized in Tri-reagent (Sigma-Aldrich) for RNA isolation.

2.4. Microarray transcriptome analysis

Four cows with follicular fluid [A4] at the highest end of the High A4 group (mean A4 = 356 ng/mL, SD = 148; range 203–597 ng/mL) and four cows with follicular fluid [A4] at the lowest end of the Control

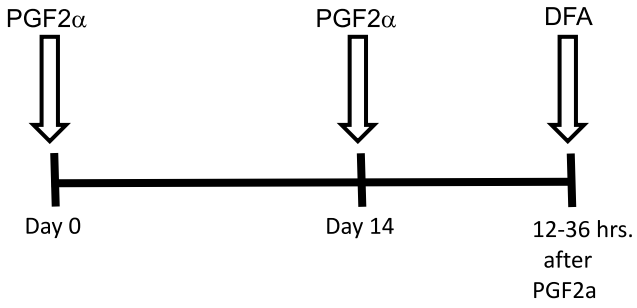

Fig. 1. Synchronization Protocol to obtain follicular fluid from dominant estrogen-active follicles to classify High A4 and Control (Low A4) cows for study. The estrous cycles of these beef cows (75% Red Angus, 25% MARC III) were synchronized with two injections of prostaglandinF2α (PGF2α) 14 days apart and transrectal ultrasound-guided ovarian follicle aspiration was performed 12–36 h after the final PGF2α injection as previously described (Summers et al., 2014).

group (mean A4 = 1.9 ng/mL, SD = 0.39; range 1.40–2.50 ng/mL) were selected for GC transcriptome analysis. After RNA extraction, 200 ng RNA for each sample (n = 4 animals for each group) were submitted to the University of Nebraska Medical Center Microarray Core facility where the Affymetrix Bovine GeneChip® Gene 1.0 ST Array RNA expression analysis was performed. Full transcriptome data is available from the NCBI GEO repository, Series GSE97017. The microarray results were normalized with Robust Multi-Array Averaging. Array analysis was then performed using the National Institute of Aging array tool (NIA) (http://lgsun.grc.nia.nih.gov/ANOVA/) for Analysis of Variance (ANOVA) to determine hierarchical clustering, and correlation between replicates. All bioinformatic analyses were performed on transcripts above a linear noise threshold of 100. Functional categorization of genes was determined by examining the gene descriptions from Entrez Gene (NCBI, http://www.ncbi.nlm.nih.gov/gene) and UniProtKB/Swiss-Prot (http://www.uniprot.org/). Predicted cell function outcomes were assessed with Ingenuity® Pathway Analysis (IPA; Winter 2016 release, Qiagen, 2021 January update). Potential miRNA targets were determined using TargetScan Release 7.1 (June 2016) for mammalian microRNAs (http://www.targetscan.org/vert_71/). The Principal Component Analysis was performed in NIA array tool (http://lgsun.grc.nia.nih.gov/ANOVA/) demonstrating the differences in High A4 and Control GCs with small and large luteal cells. Small and large luteal cells were previously compared to determine lineage differences with control GCs via NIA array and a PCA script (Romereim et al., 2016).

2.5. Quantitative real-time PCR (qPCR)

To validate the microarray results, qPCR was performed in triplicate on 384-well plates to amplify select targets from cDNA synthesized with Superscript III Reverse Transcriptase (Thermo Fisher Scientific) from the RNA samples originally used for the microarray using the primers listed in Table 1. Power SYBR™ Green Master Mix (Thermo Fisher Scientific) was utilized with an Applied Biosystems 7900HT Fast Real-Time PCR System. Expression was normalized to the geometric mean of the ribosomal RNA products RPL15 and RPL19. The results for each transcript are represented as the geometric mean of fold-changes relative to the expression of that transcript in the Control GCs.

2.6. Primary granulosa cell culture

For cell culture experiments to determine effects of A4 concentration on granulosa cells, GCs were isolated from ovaries obtained at a local abattoir (JBS, Omaha, NE). Follicles larger than 7 mm in diameter were aspirated, the follicular fluid was centrifuged (300×*g*) 10 min to pellet the GCs, and the GC pellet was digested for 15–20 min with a mixture of dispase (10 mL, Stem Cell Technologies), collagenase (final concentration of 1 mg/mL, Stem Cell Technologies), and DNase I (final concentration of 10 μg/mL, Stem Cell Technologies). The cells suspended in digestion media were then diluted with culture media (DMEM/F12 containing 2% FBS and 1% penicillin/streptomycin), counted using a Scepter 2.0 Cell Counter (EMD Millipore), and centrifuged to pellet the cells again. The cell pellet was resuspended with culture media and distributed into 6-well plates at a density of 500,000 cells per well in a 1:1 mixture of DMEM [low glucose and no phenol red or L-glutamine (11,054–001, LifeTech)] and F12 [with L-glutamine (11,765–054, LifeTech)] with 1% penicillin/streptomycin (15,140–122, LifeTech) and 2% FBS (26,140–079, LifeTech). Cells were cultured overnight (14–18 h) in this medium, and then incubated for 4 h in serum-free medium with 1% ITS supplement (51,500–056, LifeTech). The cells were then cultured with serum-free medium plus 1% ITS. Treatments were: 1) Control (PBS with no FSH or A4), 2) bovine Follicle Stimulating Hormone (0.1 IU/μL) (FSH; AFP-9294C, National Hormone and Peptide Program) reconstituted in sterile PBS; 3) FSH plus 4-androsten-3, 17-dione (A6030-000, Steraloids) reconstituted in ethanol and then diluted in PBS prior to addition to culture media at 1 nM (0.29 ng/mL); 4) FSH plus A4 at 100 nM (28.6 ng/mL); and 5) FSH plus A4 at 1 μM (286 ng/mL). Control and FSH-only media had a volume of ethanol added equivalent to that included with the highest A4 treatment (10 μL ethanol in 500 μL media). Cells were incubated with treated media for 20–22 h, and then cells were either lysed with RIPA buffer containing Halt™ protease inhibitor cocktail (78,430, Thermo Fisher Scientific) for western blots or collected for RNA isolation utilizing Tri-Reagent (Sigma) as previously described. Two collections of bovine slaughterhouse ovaries were used with three replicates per treatment for all A4 concentrations. Culture media was collected at end of culture and stored at −80 C for analysis of factors secreted in media.

2.7. Droplet digital PCR for Catenin Beta Interacting Protein 1 (CTNNBIP1)

To determine differences in gene expression of Catenin Beta Interacting Protein 1 *(CTNNBIP1),* droplet digital PCR (ddPCR) was performed in duplicate on 96-well plates to amplify select targets from cDNA synthesized with iScript Advanced (Bio-Rad) from the RNA samples collected from slaughterhouse GC cultures using the primers listed in Table 2. EvaGreen Master Mix (Bio-Rad) was used and droplets were generated utilizing DG6 cartridge (Bio-Rad) and droplet generator oil for EvaGreen Supermix (Bio-Rad). After droplets were generated, they were placed into a 96-well plate and amplified with the C1000 Touch Thermal Cycler (Bio-Rad). Once the PCR run was completed, droplets were read utilizing the QX200 Droplet reader (Bio-Rad) to count number of positive and negative droplets per sample. Concentrations were determined per sample volume and expression was normalized to 100 copies of RNA products of RPL12. A Student's t-test was used to determine differences between groups with $P < 0.05$ set for significance.

2.8. AMH ELISA

Spent culture media from GC Controls, those treated with FSH, and FSH plus A4 100 nM (28.6 ng/mL) was analyzed utilizing a commercially available bovine AMH ELISA kit (Ansh Labs, Ca# AL-114). For the analysis, culture media was not diluted and followed the manufacture's protocol. The intra-assay CV was 1.96%. A Student's t-test was utilized to determine differences between groups with $P < 0.05$ set for significance.

Table 1
qPCR Primers.

Primer	Accession Number	Forward	Reverse
CCNA2	NM_001075123.1	AAGCTGGCCTGAATCATTAGTA	TCTGAGGTAGGTCTGGTGAA
CYP17A1	NM_174304.2	GACTCCAGCATTGGCGACCT	GGGATGCTGCCACTCCTTCT
CYP19A1	NM_174305.1	TTCAACAGCAGAGAAGCTGGAA	CCACGTTTCTCAGCAAAAATCA
ECT2	NM_001097573.1	AGGAATGGCGGTAACGGTGA	ATGATGGCACTCGCAAAGGAC
RPL15	NM_001077866.1	TGGAGAGTATTGCGCCTTCTC	CACAAGTTCCACCACACTATTGG
RPL19	NM_001040516.2	CAGACGATACCGTGAATCTAAGAAGA	TGAGAATCCGCTTGTTTTTGAA

Table 2
ddPCR primers utilized for *CTNNBIP1* and *RPL12* transcripts.

Primer	Accession number	Forward	Reverse
CTNNBIP1	XM_024976736.1	TTCTTGTCAGCAAACGCAGGT	TTTGTCGCCAGAGCCAAGGT
RPL12	NM_205797.1	CCACCATGCCGCCTAAGTTC	TTTGGAGACAGACCCAGAGGGC

2.9. Western blotting and protein quantification – GC proliferation

The cell lysates in RIPA buffer plus protease inhibitors were separated by size on a 10% polyacrylamide gel using a BioRad MINI-Protean system according to the manufacturer's instructions. The separated proteins were transferred to Immobilon-FL membranes (EMD Millipore), blocked for 2 h using Odyssey® Blocking Buffer (927–40000, LI-COR), and then incubated in Odyssey® Blocking Buffer plus 1% Tween-20 and the primary antibody (rabbit anti-ACTB antibody, 4967S, Cell Signaling Technology; rabbit anti-PCNA antibody, ab29, Abcam; Table 3) overnight at 4 °C with agitation. After TBST (tris buffered saline - Tween 20) washes, blots were incubated in Odyssey® Blocking Buffer plus 1% Tween-20 plus the secondary antibody (IRDye 680CW goat anti-rabbit IgG, 926–68071, LI-COR, Table 3) for 1–2 h at room temperature with agitation. Final TBST and TBS washes were followed by blot image acquisition using the LI-COR Odyssey® CLx Imaging System. To quantify the relative amount of protein expressed in each sample, the density of each protein band in pixels was determined using ImageJ (http://imagej.nih.gov/ij/). ImageJ is a free analysis program that allows for density of protein bands to be quantitated by the number of dark pixels on a scanned image. ImageJ then was used in conjunction with the file of the blot from the LI-COR Odyssy Imaging System to quantitate protein bands using the square tool in ImageJ which measures density of pixels within the protein band. The density of the protein band for each sample was normalized using the density of ACTB and averaged over culture experiments. Data were analyzed with prism and an ANOVA was used to determine the effect of increased concentration of A4 on PCNA staining (a measure of proliferation) in granulosa cells. To determine differences between Control and dose of A4 or between A4 doses, Sidaks multiple comparisons test with planned comparisons was utilized. The main comparisons of interest were – 1) comparison of Control (non-treated GCs) vs FSH plus 1 μM A4 (286.4 ng/mL; similar to High A4 cow ff); and 2) FSH plus 1 μM A4 (286.4 ng/mL-similar to High A4 ff concentrations) vs FSH plus A4 1 nM (0.29 ng/mL; similar to Control cow ff A4 concentrations). Differences in data were considered to be statistically significant at $P \leq 0.05$.

2.10. Western blotting and protein quantification – GC signaling of granulosa cell cultures and high A4 and control cows after estrous cycle synchronization and aspiration

Granulosa cells were aspirated in dominant follicles after estrous cycle synchronization was conducted as described (Fig. 2 except no ovariectomy) to evaluate GCs from EA follicles in the naturally occurring high-androgen microenvironment compared to Controls. Transrectal ultrasound-guided follicle aspiration, rather than ovariectomy, was performed as previously described (Summers et al., 2014, Fig. 2). Aspirated samples were immediately centrifuged (300×*g*) for 10 min. After centrifugation, the follicular fluid was decanted from the resulting GC pellet. Centrifugation and decanting were repeated and GCs were then snap frozen in liquid nitrogen for western blotting.

Protein was extracted from GCs using RIPA buffer with protease inhibitors. Proteins were separated by size on a 10% polyacrylamide gel and transferred to Immobilon PVDF membranes (EMD Millipore) for protein detection. Membranes were blocked with 5% milk in TBST prior to overnight incubation with primary antibody (rabbit anti-AKT1 antibody, 9272, Cell Signaling Technology; rabbit anti-phospho-AKT antibody, 4060, Cell Signaling Technology; rabbit anti-FOXO1 antibody, ab39656, Abcam; rabbit anti-phospho-FOXO1 antibody, 9461, Cell Signaling Technology; mouse anti-CTNNB1 antibody, 610,154, BD; mouse anti-active-CTNNB1 antibody, 05–665, EMD Millipore; rabbit anti-MAPK1/3 antibody, 9102, Cell Signaling Technology; rabbit-anti-phospho-MAPK1/2; 4370, Cell Signaling Technology, Table 3). Membranes were rinsed with TBST and incubated with the secondary antibody (anti-mouse IgG, 7076, Cell Signaling Technology; anti-rabbit IgG, 7074, Cell Signaling Technology). Either SuperSignal West Pico

Table 3
Primary and secondary antibodies for western blotting.

Protein	Primary Antibody	Dilution	Substrate
ACTB	mouse monoclonal IgG_1	1:10,000	West Femto
	Cell Signaling Technology (4967S)	1:2000	West Pico
		1:500	N/A
MAPK1/3	rabbit polyclonal IgG Cell Signaling Technology (9102)	1:1000	West Pico
p-MAPK1/3	rabbit monoclonal IgG Cell Signaling Technology (4370)	1:2000	West Pico
FOXO1	rabbit polyclonal IgG Abcam (ab39656)	1:1000	West Pico
p-FOXO1	rabbit polyclonal IgG Cell Signaling Technology (9461)	1:1000	West Pico
PCNA	mouse monoclonal IgG Abcam (ab29)	1:1000	N/A
p-AKT1	rabbit monoclonal IgG	1:8000	West Femto
	Cell Signaling Technology (4060)		
CTNNB1	mouse monoclonal IgG_1	1:8000	West Femto
	BD Transduction Laboratory (610,154)		
Non-p-CTNNB1	mouse monoclonal IgG_{1K}	1:8000	West Femto
	Millipore (05–665)		
Specificity	**Secondary Antibody**	**Dilution**	**Substrate**
anti-mouse	horseradish peroxidase-linked IgG Cell Signaling Technology (7076)	1:10,000	West Femto
		1:20,000 (with ACTB 1° Ab)	
		1:2000	West Pico
Anti-rabbit	horseradish peroxidase-linked IgG Cell Signaling Technology (7074)	1:10,000	West Femto
		1:2000	West Pico
Anti-rabbit	IRDye 680CW IgG LI-COR (926–68071)	1:5000	N/A

ACTB = actin, beta; AKT1 = v-akt murine thymoma viral oncogene homolog 1; CTNNB1 = beta catenin; MAPK1/3 = mitogen-activated protein kinase 1 and 3; FOXO1 = forkhead box O1; PCNA = proliferating cell nuclear antigen; p = phosphorylated.

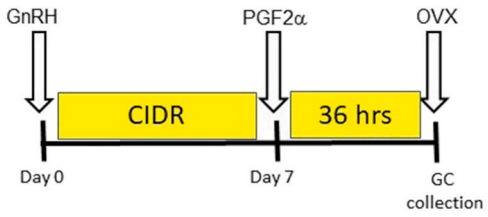

Fig. 2. Synchronization protocol for obtaining granulosa cells for microarray analysis in the High A4 and Control groups. Estrous cycles of cows were synchronized with a modified Co-Synch protocol using gonadotropin releasing hormone (GnRH) and a controlled internal drug release device (CIDR; 1.38 g progesterone, Zoetis) for 7 days with a PGF2α (25 mg/mL; Lutalyse, Zoetis) injection at CIDR removal (Summers et al., 2014). This protocol was utilized so all follicle waves that developed would be more synchronized and the dominant follicles would be at similar stages of development to allow for less variation with gene expression in individual follicles from each cow for the microarray analysis.

Chemiluminesent Substrate (Pierce) (FOXO1, phospho-FOXO1, MAPK1/3, phospho-MAPK1/3, Table 3) or SuperSignal West Femto Maximum Sensitivity Substrate (Pierce) (AKT1, phosphor-AKT1, CTNNB1, active-CTNNB1, Table 3) was added to the membranes and protein bands were visualized following exposure on x-ray film.

Following initial transfer, blots were stripped with Restore Western Blot Stripping Buffer (Pierce), re-blocked, and incubated with a mouse monoclonal primary antibody against beta actin (mouse anti-ACTB antibody, 4967, Cell Signaling Technology, Table 3). Following a TBST rinse, membranes were incubated with the secondary antibody (anti-mouse IgG, 7076, Cell Signaling Technology, Table 3) and protein bands were visualized as previously described. Quantification was conducted as described above except band density was measured using Adobe Photoshop. A Student's *t*-test was used to compare means among three different experiments; differences in data was considered to be statistically significant at $P \leq 0.05$.

2.11. Collection and fixation of GCs after FSH stimulation

To obtain histology from GCs in EA follicles from Control and High A4 cows, estrous cycles were synchronized and stimulated with FSH (Fig. 3).

Aspirates were centrifuged to remove ff from granulosa cells and pellets were resuspended with PBS. After the cell pellet was suspended, aliquots of 10^5 GCs (n = 4 replicates per animal) were placed on ice and washed twice with 2% FCS-PBS. Cell pellets were diluted in 100 μl chilled 1% BSA-PBS. Cytospin slides were prepared based on manufacturer's instructions (Statspin CytoFuge 2, HemoCue America). Diluted cells were aliquoted 100 μl in to each well, the lid was placed over the samples and spun at maximum speed (1060×*g*) for 2 min. Filters were gently removed from slides to prevent smearing and slides were examined to ensure cells annealed properly. Slides were then dried in a desiccation chamber overnight.

2.12. Collection and fixation of antral follicles

For histology of ovarian follicles, antral follicles (>7 mm diameter) were isolated from ovaries obtained at a local abattoir (JBS, Omaha, NE). Isolated follicles were placed in chilled 4% paraformaldehyde and fixed overnight at 4 °C rocking. Follicles were then washed 3 times with 1x PBS for 5 min at 4 °C rocking and then incubated overnight in 1x PBS containing 30% sucrose at 4 °C rocking. The following day, half of the sucrose solution was removed and an equal volume of Optimal Cutting Temperature (OCT) compound (Thermo Fisher Scientific) was added and the tissue was incubated for 3 h at 4 °C rocking. Follicles were then arranged at the bottom of a plastic mold filled with OCT and placed in a mixture of dry ice and 70% ethanol to allow the samples to freeze. All embedded samples were then stored at −80 °C until sectioning. Follicles were sectioned at a thickness of 20 μm and mounted on slides for immunostaining.

2.13. Follicle and GC immunohistochemistry for steroidogenic enzymes

For immunohistochemistry of FSH stimulated GCs from High A4 and Control cows and slaughterhouse follicles, sections and cells were fixed with 4% paraformaldehyde for 10 min at room temperature. Slides were washed three times for 5 min in 1x PBS and then permeabilized with 0.1% Tween-20 in PBS for 10 min. Slides were then washed for 5 min with 1x PBS, then blocked in 30% BSA in PBST (0.05% Tween-20 in 1x PBS) for 80 min at room temperature. Slides were incubated with a primary antibody (mouse anti-aromatase, 1:100, ab139492, Abcam; rabbit anti-CY17A1, 1:50, ABC 392 EMD Millipore) in 3% BSA in PBST overnight at 4 °C. Slides were washed 5 times for 5 min with 1x PBST and then incubated with a secondary antibody (Alexa Fluor 555 goat anti-mouse IgG, 1:1000, Thermo Fisher Scientific; Alexa Fluor 488 donkey anti-rabbit IgG, 1:1000, A21206, Thermo Fisher Scientific) in 3% BSA in PBST for 2.5 h. Slides were washed 3 times for 5 min in 1x PBST, incubated with DAPI (5 ng/mL) in 1x PBS for 5 min and then washed 3 times for 5 min with PBS. Slides were mounted with Prolong Gold with Antifade (Thermo Fisher Scientific) and sealed. Slides were imaged at the University of Nebraska-Lincoln Microscopy Core using the Olympus FV3000 laser scanning confocal microscope. Localization of CYP17A1 and CYP19A1 was quantified using ImageJ and approximate percentages were reported for granulosa cell staining.

3. Results

3.1. A high-androgen follicular microenvironment generates differentially regulated transcripts in granulosa cells

During a multi-year, multiple estrous cycle survey to classify bovine reproductive phenotypes, the GCs and follicular fluid from dominant follicles were isolated (Summers et al., 2014). The purity of GCs was determined using immunofluorescence (IF) against smooth muscle actin, which is a marker for contaminating theca cells (≥94% in our preparation) (Romereim et al., 2016). Based on the previously published

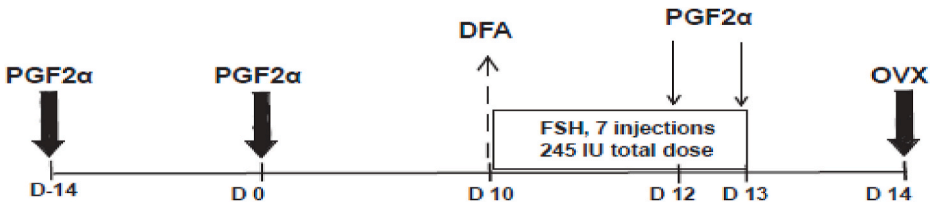

Fig. 3. Synchronization protocol to stimulate GCs *in vivo* with FSH and develop multiple follicles to obtain GCs. Cow estrous cycles were synchronized to collect GCs after FSH for histology via a cytospin centrifuge allowing for individual cells to be adhered onto slides and the identification of multiple co-labeled steroid enzyme antibodies. Cows were administered two PGF2α injections 14 days apart, transrectal ultrasound-guided aspiration of the dominant follicle was performed (Summers et al., 2014) on day 10 after the last PGF2α to allow for increased follicles to develop (and increased GCs) in response to FSH. Immediately after, a series of FSH injections (20 mg/mL injection; 140 mg/mL total; Folltropin-V, Vetoquinol) were given 12 h apart over a 4-day period. On day 12 and 13 of the protocol, PGF2α was administered to stimulate regression of any luteal tissue and allow for continued development of antral follicles. Ovariectomy (Youngquist et al., 1995) was performed approximately 24 h after the last PGF2α injection and all antral follicles larger than 7 mm in diameter were aspirated.

classifications of the androgen content of the follicular fluid (Summers et al., 2014), GC samples were selected and utilized for Affymetrix RNA microarray analysis [NCBI GEO GSE97017]. Hierarchical clustering of overall transcriptomes demonstrated that GCs can be distinguished by the androgen content of their follicle-of-origin (Fig. 4A). While the Control or High A4 status of the GCs can be determined by their transcriptomes, the list of differentially regulated transcripts between the two categories is surprisingly limited once statistical thresholds ($P < 0.005$, false discovery rate (FDR) < 0.05, linear noise threshold of 100) are applied and unannotated probes are omitted, leaving 60 upregulated transcripts and 210 downregulated transcripts (Data in Brief, Snider et al., XXXXXXXX). The differentially regulated transcripts with highest fold-changes between High A4 and Control GCs are shown in Table 4. A full list of the differentially expressed genes can be found in Snider et al. XXXXXXX (Data in Brief). Select genes were validated by qPCR (Fig. 4B). We also previously validated differential expression of several genes between control GCs and other ovarian somatic cells (Romereim et al., 2016).

3.2. High-A4 microenvironment results in decreased expression of proliferation markers

The differentially regulated transcripts of the High A4 GCs compared to the Control GCs provided insights regarding functional differences between the two sets of cells. Using the Ingenuity Pathway Analysis (IPA) software, a list of predicted networks with functional significance in High A4 compared to control granulosa cells were identified (Table 5). The predictions suggested that the High A4 GCs had inhibited proliferation, cell cycle progress, and cell survival compared to the Control GCs. These IPA predictions were supported by the assessment of the functional annotations of all the differentially regulated genes based on Entrez and UniProKB databases. The categories with the highest representation, based on the 60 upregulated mRNAs, were miRNA, cell signaling, and immune function genes (Fig. 5A). The most represented categories, based on the 210 downregulated genes, were those involved in mitosis and the cell cycle, cellular metabolism, and transcription regulation (Fig. 5B).

To confirm that reduced GC proliferation (the main predicted outcome for High A4 GCs) was due to the excess A4 in the follicular fluid rather than some other variable, primary GCs obtained from large antral follicles of ovaries from a local abattoir were cultured and treated with control media, bovine FSH, or bovine FSH and one of three concentrations of A4. The lowest concentration of A4 is on the same order of magnitude as the A4 content of the follicular fluid of the Control cows (0.29 ng/mL or 1 nM), while the highest concentration of A4 is on the same scale as the highest A4 content of follicles from High A4 cows (286 ng/mL or 1 μM). After 20–22 h of treatment with FSH and/or A4, Western blot was performed to quantify the proliferation marker PCNA normalized to beta actin (ACTB) (Fig. 6). Treatment with A4 caused reduced PCNA in granulosa cells treated with FSH plus 1 μM (290 ng/mL) of A4 compared to FSH plus 1 nM (0.29 ng/mL) A4 similar to that found in Control cows. Also the GCs treated with FSH plus 1 μM (286 ng/mL) also had reduced PCNA when compared to GCs with no FSH or A4 treatment (Fig. 6).

3.3. Potential regulators of inhibition of granulosa proliferation

The IPA software was used to predict changes in upstream regulators (activation or inhibition) based on the expression differences observed in target downstream genes. Based on the differentially regulated transcripts in the High A4 GCs compared to the Control GCs, potential upstream regulators of inhibited cell proliferation were identified (Data in Brief, Snider et al., XXXX). Additionally, this analysis was used to uncover possible regulatory mechanisms that could be driving the transcriptome changes in the High A4 GCs.

Several predicted miRNAs that may regulate the expression of differentially regulated genes in High A4 granulosa cells were identified. Ten miRNAs were upregulated in the High A4 GCs, and one miRNA was downregulated (Table 6; with fold expression values identified in microarray analysis, NIA array tool and IPA). Using TargetScan, 118 downregulated mRNAs (112 annotated) from the microarray analysis were predicted as targets of the upregulated miRNAs (Data in Brief, Snider et al., XXXX). Many of these miRNAs can potentially regulate more than one mRNA transcripts. The functions of these 112 annotated genes are primarily associated with mitosis and the cell cycle, metabolism, and transcription regulation (Fig. 7).

3.4. High-A4 microenvironment resulted in altered signaling pathway activation

Slaughterhouse GC's treated with 100 nM A4 compared to controls (182.0 ± 4.59 vs 146.0 ± 5.68 pg/mL, respectively) (Fig. 8A) had increased AMH production. AMH produced from GCs can inhibit Wingless-type mouse mammary tumor virus integration site (WNT) signaling pathway by production of *CTNNBIP1* (Zhang et al., 2015). The WNT signaling pathway is one of the major established cellular proliferation pathways. This pathway was therefore investigated in slaughterhouse GCs treated with increased concentrations of A4 to that in High A4 cow follicular fluid. We also evaluated mRNA abundance of *CTNNBIP1* since this molecule inhibits active beta catenin from

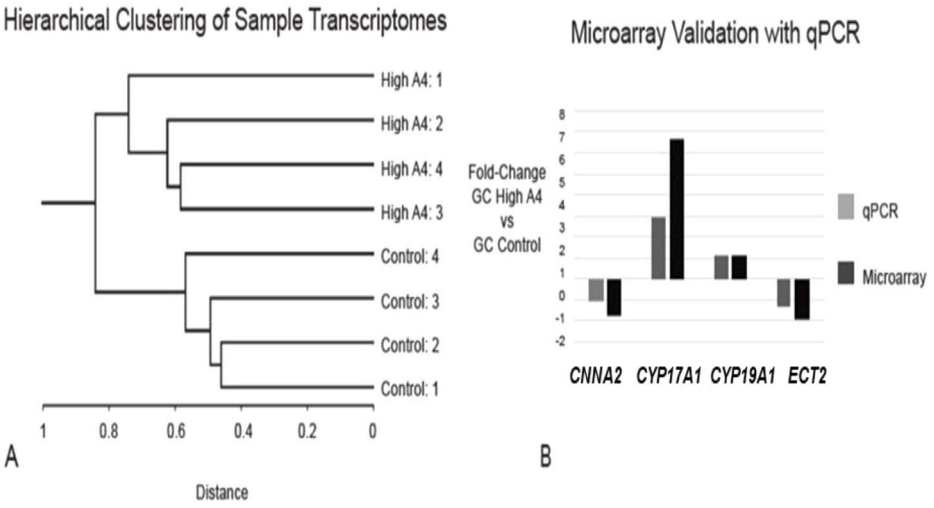

Fig. 4. Transcriptome comparison between High and Control GCs. (A) Hierarchical clustering of the transcriptomes identified that the High A4 GCs cluster together and the Control GCs cluster together. The distance along the x-axis at which each branching point occurs represents how similar or dissimilar each sample is, with more similar samples branching closer to 0. (B) Microarray validation using qPCR shows that the fold-changes for *CCNA2*, *CYP17A1*, and *ECT2* are of similar magnitude, while *CYP19A1* is not different using either method.

Table 4
Select Differentially Regulated Genes in High A4 vs. Control Granulosa Cells.

Probeset ID	Gene Symbol	Description	Fold Change	Control Avg Expression	High A4 Avg Expression	Location	Family	Function
12900052	*TAAR6*	trace amine associated receptor 6	6.98	13.71	105.88	Plasma Membrane	G-protein coupled receptor	Signaling
12821429	*CYP17A1*	cytochrome P450 family 17 subfamily A member 1	6.65	103.71	622.87	Cytoplasm	Enzyme	Steroidogenesis
12862676	*TAS2R10*	taste 2 receptor member 10	3.45	32.39	108.71	Plasma Membrane	G-protein coupled receptor	Signaling
12892676	*ALDH1A1*	aldehyde dehydrogenase 1 family member A1	3.19	51.63	188.81	Cytoplasm	Enzyme	Metabolism
12822732	*CHST15*	carbohydrate sulfotransferase 15	2.53	274.23	711.00	Plasma Membrane	Enzyme	Extracellular matrix
12819205	*AS3MT*	arsenite methyltransferase	2.50	64.51	150.39	Cytoplasm	Enzyme	Metabolism
12834667	*PRSS23*	protease, serine 23	2.33	662.65	1540.76	Extracellular Space	Peptidase	Signaling
12751697	*NDRG4*	NDRG family member 4	2.32	314.15	719.73	Plasma Membrane	Other	Signaling
12680976	*ATP13A3*	ATPase 13A3	2.14	756.15	1569.44	Extracellular Space	transporter	Ion transport
12846005	*TTF2*	transcription termination factor 2	−2.01	127.55	63.38	Cytoplasm	transcription regulator	Transcription and transcription regulation
12796835	*KIF15*	kinesin family member 15	−2.04	254.74	133.83	Nucleus	Other	Mitosis
12808472	*NDC80*	NDC80, kinetochore complex component	−2.08	359.29	175.67	Nucleus	Other	Mitosis
12755848	*SLC7A5*	solute carrier family 7 member 5	−2.09	127.48	64.86	Plasma Membrane	transporter	Molecular transport
12802644	*HIST1H4B*	histone cluster 1 H4 family member b	−2.12	169.43	84.69	Nucleus	Other	Chromatin structure
12740526	*NPHS2*	NPHS2, podocin	−2.13	126.72	56.27	Plasma Membrane	Other	Protein-protein binding
12780541	*IGFBP5*	insulin like growth factor binding protein 5	−2.13	114.88	53.06	Extracellular Space	Other	Signaling
12722357	*FBXO32*	F-box protein 32	−2.15	153.06	81.06	Cytoplasm	Enzyme	Protein degradation
12718797	*DSN1*	DSN1 homolog, MIS12 kinetochore complex component	−2.17	152.07	73.77	Nucleus	Other	Mitosis
12876902	*HMMR*	hyaluronan mediated motility receptor	−2.17	333.82	154.25	Plasma Membrane	transmembrane receptor	Signaling
12862370	*PARPBP*	PARP1 binding protein	−2.18	152.05	71.86	Nucleus	Other	DNA repair
12871525	*NCAPG*	non-SMC condensin I complex subunit G	−2.21	578.57	269.15	Nucleus	Other	Mitosis
12898870	*PRSS35*	protease, serine 35	−2.23	174.20	76.46	Extracellular Space	Peptidase	Signaling
12825587	*CENPU*	centromere protein U	−2.30	269.11	119.63	Nucleus	Other	Chromatin structure
12692009	*NUSAP1*	nucleolar and spindle associated protein 1	−2.32	147.90	60.04	Nucleus	Other	Mitosis
12805984	*GMNN*	geminin, DNA replication inhibitor	−2.34	121.91	51.56	Nucleus	transcription regulator	DNA replication
12745867	*KNTC1*	kinetochore associated 1	−2.35	329.52	144.28	Nucleus	Other	Mitosis
12835737	*JUN*	Jun proto-oncogene, AP-1 transcription factor subunit	−2.36	482.69	208.88	Nucleus	transcription regulator	Transcription and transcription regulation
12815755	*KIF22*	kinesin family member 22	−2.39	144.64	56.69	Nucleus	Other	Mitosis
12843247	*PHGDH*	phosphoglycerate dehydrogenase	−2.45	168.49	71.12	Cytoplasm	Enzyme	Metabolism
12894921	*ESCO2*	establishment of sister chromatid cohesion N-acetyltransferase 2	−2.54	466.64	189.13	Nucleus	Enzyme	Mitosis
12877406	*EGR1*	early growth response 1	−2.83	700.86	253.77	Nucleus	transcription regulator	Transcription and transcription regulation
12802519	*HIST1H2BM*	histone cluster 1 H2B family member m	−2.87	1055.36	397.45	Nucleus	Other	Chromatin structure
12687887	*FOS*	Fos proto-oncogene, AP-1 transcription factor subunit	−3.09	161.23	48.81	Nucleus	transcription regulator	Transcription and transcription regulation
12905574	*DYNLT3*	dynein light chain Tctex-type 3	−3.13	121.89	39.77	Cytoplasm	Other	Molecular transport
12774842	*AOX1*	aldehyde oxidase 1	−3.30	274.91	81.15	Cytoplasm	Enzyme	Metabolism
12761259	*SUMO2*	small ubiquitin-like modifier 2	−5.21	955.58	222.36	Nucleus	Enzyme	Posttranslational modification

interacting with TCF downstream of WNT signaling. Increased *CTNNBIP1* has been shown to cause cell cycle arrest and apoptosis in certain cancers (Park et al., 2017). When GCs were treated with A4, there was increased expression of mRNA abundance of *CTNNBIP1* compared to controls (Fig. 8B).

Using Western blot analysis, the abundance of signal transduction pathway proteins that regulate cell proliferation were measured in GCs from EA dominant follicles, relative to ACTB. Non-phosphorylated CTNNB1 (active beta catenin) ($P < 0.02$) was greater in High A4 GCs (n = 9) compared to Control GCs (n = 17) (Fig. 8C) but no significant

Table 5
Ingenuity pathway analysis predicted inhibited functions based on all differentially up and down regulated granulosa cell genes.

Predicted Inhibited Functions in High A4 GCs	p-Value	# Molecules
Alignment of chromosomes	1.42E-14	11
Cell survival	2.34E-04	43
Cell viability	2.36E-04	41
Cytokinesis	1.45E-07	15
Interphase	3.10E-07	31
M phase	1.85E-11	22
Proliferation of cells	2.02E-04	93
Repair of cells	1.91E-03	6
Repair of DNA	1.16E-06	18

differences were identified in relative protein abundance for phosphorylated (inactive) CTNNB1, AKT1 (v-akt murine thymoma viral oncogene homolog 1; also known as protein kinase B), phosphorylated AKT1, FOXO1 (forkhead box O1), phosphorylated FOXO1, MAPK1/3 and MAPK1/3 (mitogen-activated protein kinase 1 and 3; also known as ERK2 and ERK1), or phosphorylated MAPK1/3. There is the potential for increased CTNNBIP1 protein to block WNT signaling, causing cell cycle arrest or decreased proliferation. The increase in active beta catenin (Fig. 8C) may be a compensatory mechanism to increase available substrate to promote granulosa cell survival.

3.5. Comparison of high A4 GCs and luteal cell transcriptomes

One major driver of gene expression profile change in GCs is the luteinization process. To determine whether GCs in the High A4 follicles were undergoing premature luteinization or other changes in their cellular function, Principal Component Analysis (PCA) was performed on the transcriptomes of the High A4 GCs, the Control GCs, and previously published microarray data from large luteal cells (LLCs) and small luteal cells (SLCs) (Fig. 9A) (Romereim et al., 2016). A graph of Principal Component 1 (PC1, including 83.45% of the variance) on the X-axis and PC2 on the Y-axis, shows that the distribution of the High A4 GCs along the x-axis is shifted towards right falling between Control GCs and the LLCs and SLCs; although, some of the High A4 GCs and Control GCs overlap (Fig. 9B).

While the High A4 GCs do not cluster with either of the luteal cell populations, a modest shift, suggests some luteal cell-like gene expression patterns. Therefore, we compared gene expression in High A4 granulosa cells with our previously published PCA data that identified genes that are enriched in LLCs or SLCs as well as genes common to either the follicular cells (TCs and GCs) or luteal cells (LLCs and SLCs) (Romereim et al., 2016). None of the genes specifically enriched in LLCs or SLCs had significantly increased expression in the High A4 GCs compared to the Control GCs. Also, there are only three genes that are enriched in TCs that are significantly increased in expression in the High

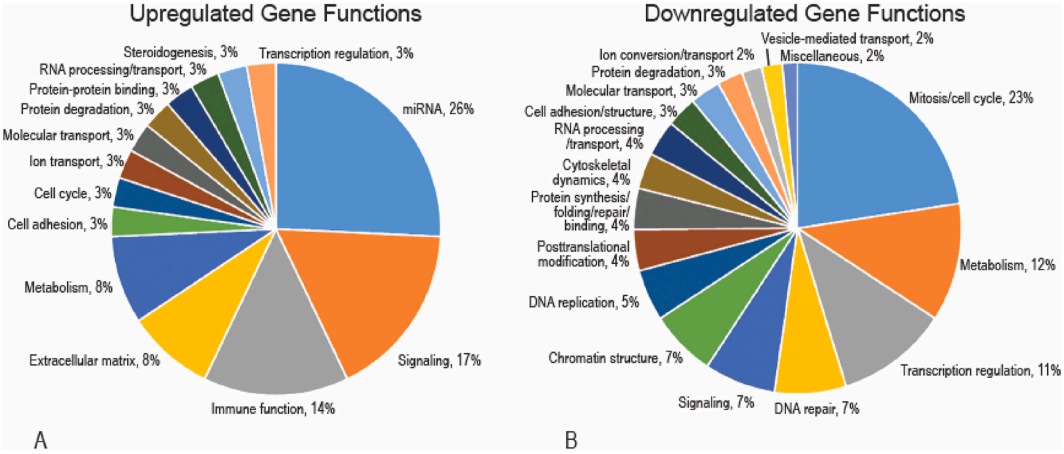

Fig. 5. Functions of differentially regulated genes. The functions of each differentially regulated gene as determined by Entrez and UniProt/KB annotations for (A) the 60 upregulated transcripts in the High A4 GCs and (B) the 210 downregulated transcripts in the High A4 GCs compared to the Control GCs.

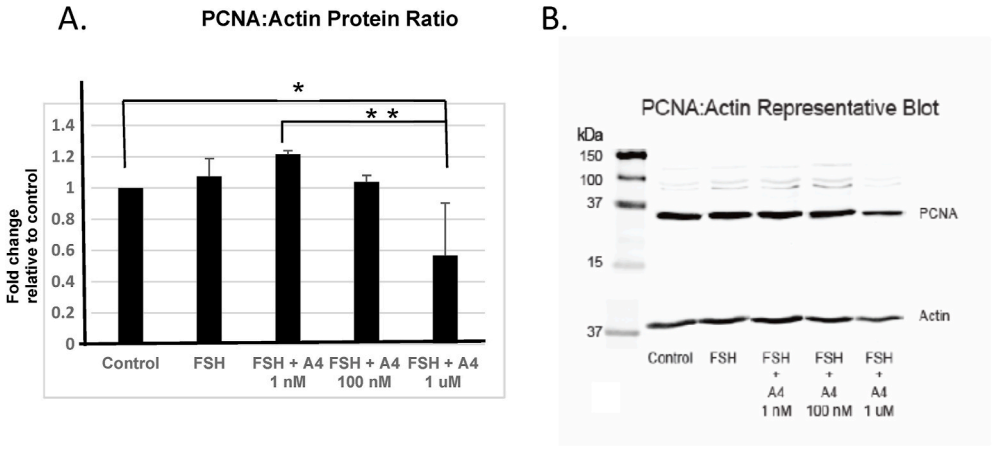

Fig. 6. Western blot quantification of GC proliferation in cell culture. Primary GCs pooled from large antral follicles of unclassified ovaries were cultured overnight and then treated with basal media, FSH (0.1 IU/μL), or FSH and the indicated A4 concentrations for 22 h (n = 3 wells per treatment X 2 slaughterhouse collections). An ANOVA demonstrated an effect of androgen on PCNA expression ($P \leq 0.05$) (A) Western blot quantification of the proliferation marker PCNA normalized to beta actin shows that FSH plus 1uM of A4 (286 ng/mL; scale of A4 observed in High A4 cow dominant follicle ff) suppressed PCNA protein detected in GCs indicating reduced proliferation compared to GCs with no treatment. Furthermore, FSH plus 1uM A4 (286 ng/mL) had reduced PCNA when compared to FSH plus 1 nM A4 (scale of A4 observed in Control cow dominant follicle ff). (B) A representative blot is shown. $^{*}P < 0.04$, $^{**}P < 0.01$.

Table 6
Differentially Regulated miRNA in High A4 vs. Control Granulosa Cells.

Probeset ID	Gene Symbol	Conserved miRNA Family	Description	Fold Change	Control GC Average	High A4 GC Average
12906595	*MIR105A*	miR-105–5p (and other miRNAs w/seed CAAAUGC)	bta-mir-105a	2.18	209.86	437.09
12791562	*MIR211*	miR-204–5p (and other miRNAs w/seed UCCCUUU)	bta-mir-211	2.20	86.41	171.53
12774048	*MIR2358*	Bovine-only, no known conserved family	bta-mir-2358	−1.57	203.90	129.74
12788834	*MIR2364*	Bovine-only, no known conserved family	bta-mir-2364	1.81	266.92	478.13
12856465	*MIR2427*	Bovine-only, no known conserved family	bta-mir-2427	1.76	156.55	276.90
12896347	*MIR2481*	Bovine-only, no known conserved family	bta-mir-2481	1.60	110.71	177.06
12730564	*MIR326*	miR-330–5p (and other miRNAs w/seed CUCUGGG)	bta-mir-326	1.78	83.98	132.86
12784970	*MIR449B*	miR-34a-5p (and other miRNAs w/seed GGCAGUG)	bta-mir-449b	1.72	104.73	181.11
12832475	*MIR449D*	Bovine-only, no known conserved family	bta-mir-449d	1.58	103.75	152.47
12829226	*MIR483*	miR-483–3p (miRNAs w/seed CACUCCU)	bta-mir-483	1.64	120.87	194.30
12829236	*MIR584-7*	miR-584–5p (and other miRNAs w/seed UAUGGUU)	bta-mir-584-7	1.87	82.68	147.75

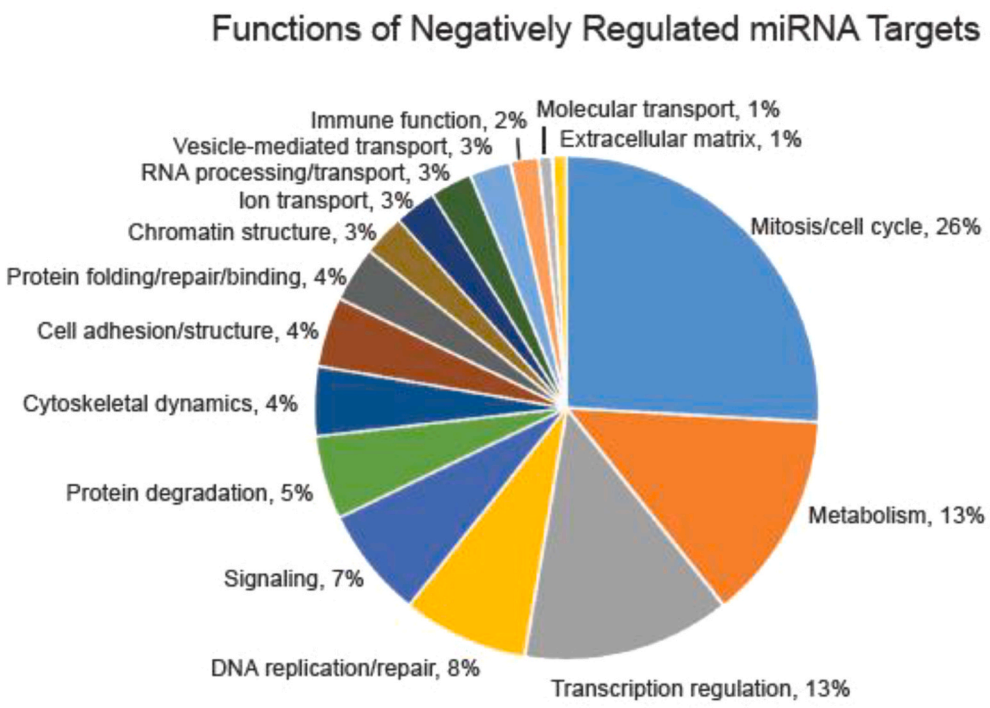

Fig. 7. Functions of predicted miRNA targets that are differentially regulated in High A4 GCs. The miRNAs, which were upregulated in High A4 GCs, had 112 unique potential mRNA targets that were identified as differentially expressed in the microarray analysis. The functions of these mRNA targets as determined by Entrez and UniProt/KB annotations are shown.

A4 GCs (*COL4A1*, *AS3MT*, and *CYP17A1*; Table 7).

However, there are several transcripts that are enriched in GCs are differentially expressed in High A4 GCs (Data in Brief, Snider et al., XXXXXXXX). Two of these transcripts (*NDRG4* and *UNC79*) had the highest expression in the High A4 GCs compared to all other cell types (luteal, thecal). Three transcripts (*IGFBP5*, *SQRDL*, and *CYBRD1*) had the lowest expression in the High A4 GCs compared to other cell types-Control GC, luteal and thecal). All other genes were significantly lower in the High A4 GCs than the Control GCs, which could lead to a shift towards the expression levels seen in TCs, LLCs, and SLCs. This includes the loss of expression of one of the suggested GC-specific markers: RGS17 in High A4 GCs compared to Control GCs (Data in Brief, Snider et al., XXXXXXXX). Interestingly, there were 74 differentially expressed genes in High A4 GCs that were identified as enriched in luteal cell types but not in follicular cells (Control GC and thecal). Alternatively, there were 17 genes differentially expressed in High A4 GCs that are enriched in follicular compared to luteal cells. Additionally, most of the genes indicating a High A4 GC shift towards a luteal expression pattern were those involved with mitosis and the cell cycle.

3.6. Localization of CYP17A1 and CYP19A1 expression in bovine ovarian follicles

Because *in vivo* and in vitro data showed that excess androgens inhibit cell proliferation, and because there was increased CYP17A1 in High A4 granulosa cells, localization of enzymes that regulate androgens (CYP17A1) and estrogens (CYP19A1) were determined using immunofluorescence. GCs from large antral follicles (>10 mm diameter) from 3 cows classified as Control and 3 cows classified as High A4 were collected after FSH stimulation, affixed to slides via a Cytospin centrifuge, and immunofluorescence was performed using antibodies against both CYP17A1 and CYP19A1. Although expression of aromatase (CYP19A1) in GCs was expected, expression of CYP17A1 was also present within GCs, independent of their androgen classification (High A4 or Control) (Fig. 10). To verify the presence of CYP17A1 protein in bovine GCs, immunofluorescence was also conducted in large antral follicles (>7 mm diameter, n = 3) isolated from un-classified ovaries obtained from cows at a local abattoir. As expected, CYP17A1 expression was localized to theca cells and CYP19A1 was localized to granulosa cells. Unexpectedly, CYP17A1 expression was also localized to GCs within antral follicles (Fig. 11). Based on the staining, there was

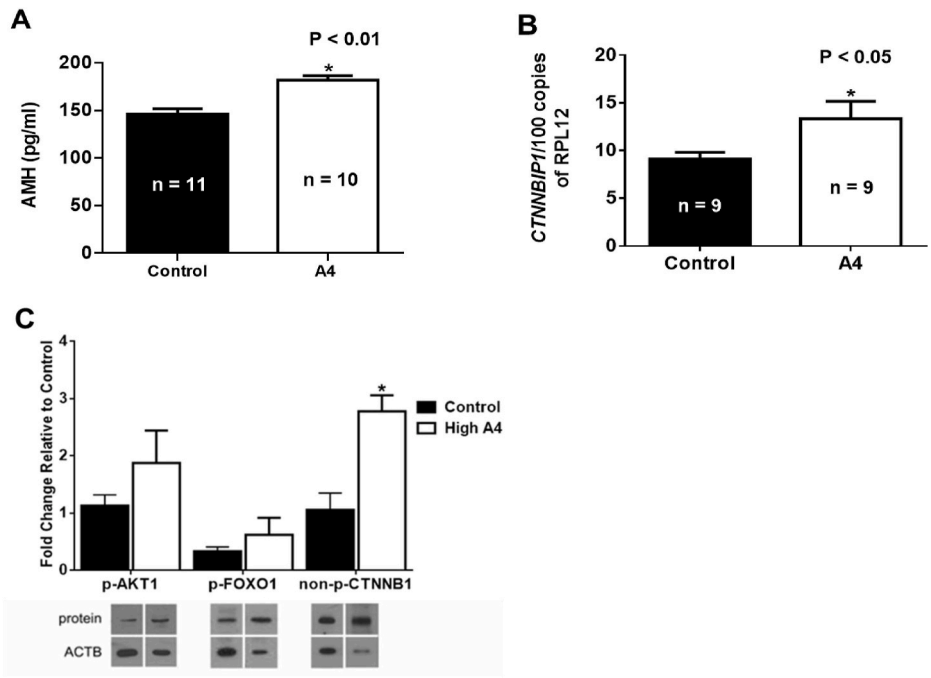

Fig. 8. Altered expression of markers involved in the WNT signaling pathway in High and Control GCs. Primary GCs pooled from large antral follicles of un-classified ovaries were cultured overnight and then treated with media containing FSH (0.1 IU/μL) as the control or with A4 (100 nM) as the treatment. (A) ELISA-quantified AMH concentrations in GC culture media increased in A4 treatment conditions compared to controls. (B) *CTNNBIP1* expression was measured in GCs by ddPCR, and *CTNNBIP1* expression was increased in A4-treated GCs compared to controls. (C) Western blot analysis was conducted to detect protein levels for GCs from dominant, EA follicles. Beta actin (ACTB) was used as an endogenous control. Means were compared between GCs classified as High A4 (n = 9) and Control (n = 17). Significant increased protein expression of non-p-CTNNB1 was observed in High A4 GCs compared to controls. *$P < 0.05$. p = phosphorylated.

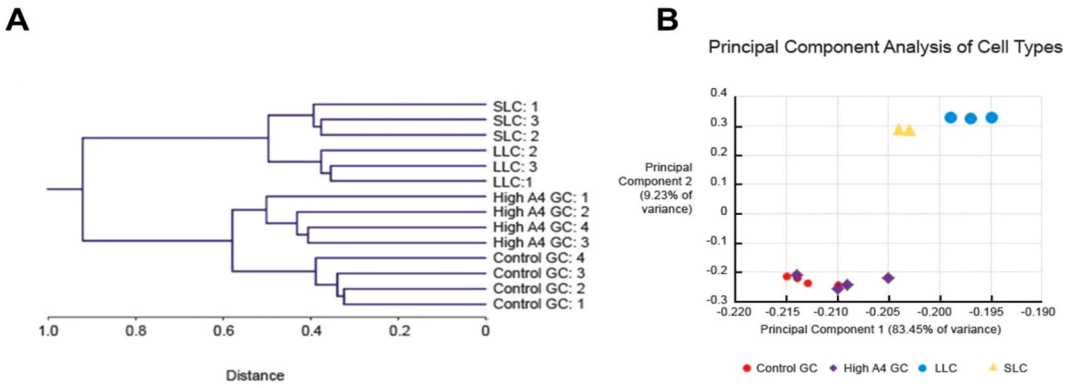

Fig. 9. Principal Component Analysis and Hierarchical Clustering of High and Control GCs compared to luteal cells. (A) Hierarchical clustering of the individual samples within each cell type/group shows that SLCs and LLCs are similar to each other though distinguishable as a cell type, just as High A4 GCs and Control GCs are similar but distinct. (B) The Eigenvalues for Principal Component 1 and Principal Component 2 are graphically represented to show the variability between samples. The LLCs and SLCs (transcriptomes previously published in Romereim et al., 2016) cluster by cell type. The Control GCs and High A4 GCs overlap, though the High A4 GCs are shifted towards the luteal cells based on Principal Component 1.

Table 7
Theca cell enriched genes with increased expression in high A4 GCs.

Probe Set ID	Gene	Description	Fold Change (High A4 GC vs Control GC)	Expression Pattern Shift	Functional Category	Fold Change (LLC vs GC)	Fold Change (LLC vs TC)	Fold Change (LLC vs SLC)
12711158	*COL4A1*	collagen type IV alpha 1 chain	1.588	Towards TC	extracellular matrix	2.13	2.736	3.405
12819205	*AS3MT*	arsenite methyltransferase	2.497	Towards TC	metabolism	6.129	21.453	6.709
12821429	*CYP17A1*	cytochrome P450 family 17 subfamily A member 1	6.649	Towards TC	steroidogenesis	11.595	129.714	37.024

approximately 45% CYP17A1 and 55% CYP19A1 expression in granulosa cells from the large antral follicles.

4. Discussion

4.1. Transcriptomes of granulosa cells are distinguishable by the androstenedione content of the follicular microenvironment

Hierarchical clustering clearly distinguishes the transcriptomes of

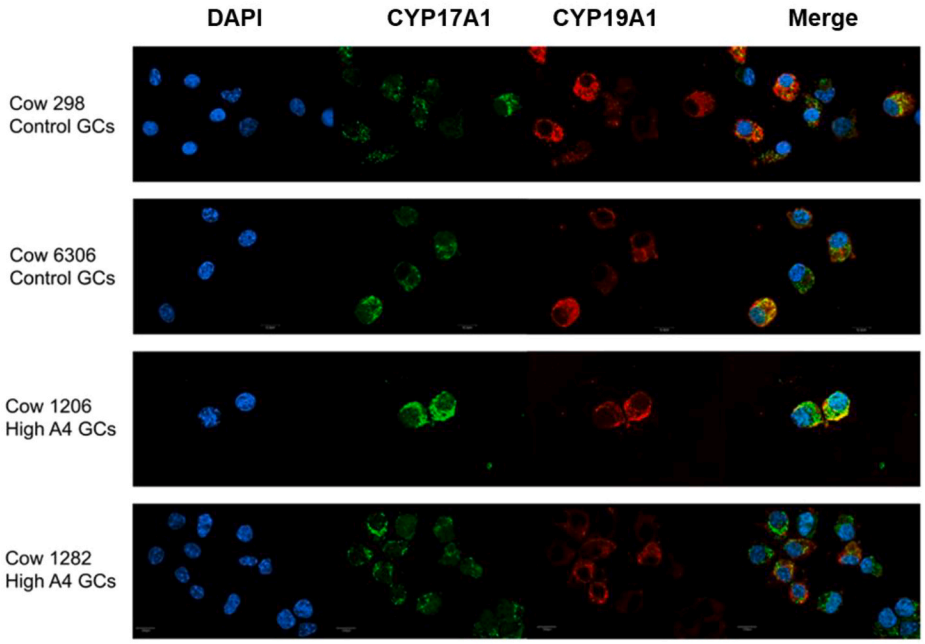

Fig. 10. CYP17A1 and CYP19A1 in bovine High A4 and Control GCs. Representative images of immunostaining for DAPI to identify nuclei (blue), as well as CYP17A1 (green) and CYP19A1 (red) expression in GCs aspirated from large antral follicles (>10 mm diameter) of cows classified as Control (n = 3) or High A4 (n = 3) after FSH stimulation (Fig. 3). Merged images identify locations with dual CYP17A1 and CYP19A1 expression (yellow). Scale bar represents 10 μm.

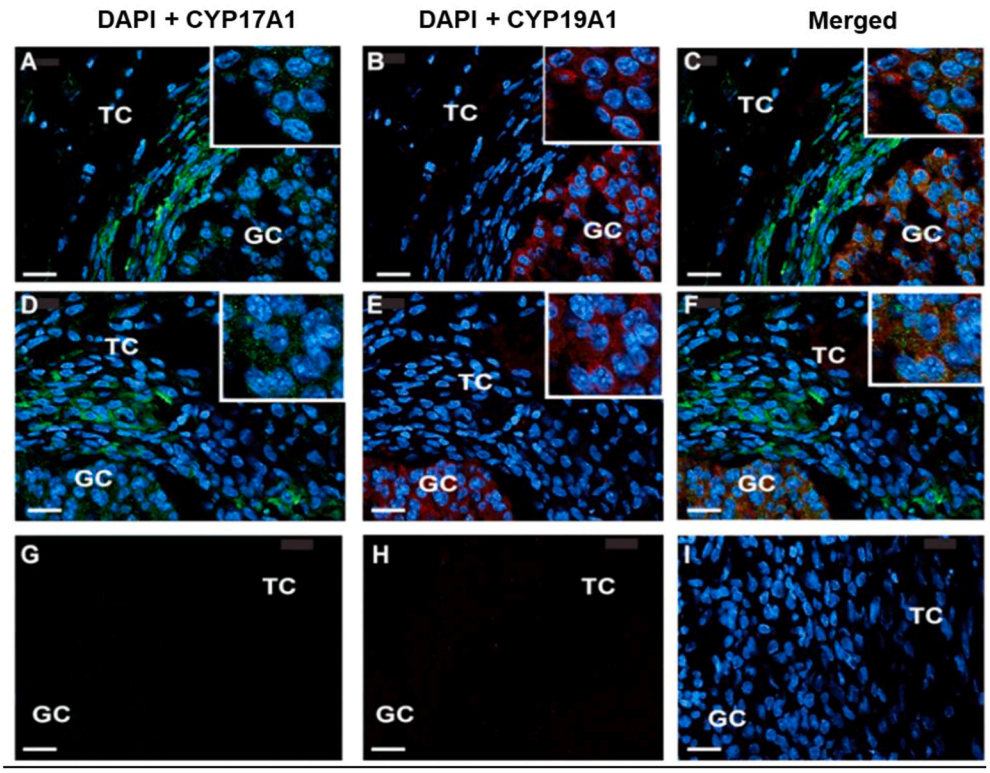

Fig. 11. Localization of CYP17A1 and CYP19A1 expression in bovine ovarian follicles. Representative images of immunostaining for DAPI to identify nuclei (blue), as well as CYP17A1 (green) and CYP19A1 (red) expression in large antral follicles (>7 mm diameter) isolated from the ovaries of unclassified cows collected at a local abattoir (n = 3). There was approximately 45% CYP17A1 and 55% CYP19A1 expression in granulosa cells. Scale bar represents 20 μm. GC, granulosa cells; TC, theca cells.

GCs of preovulatory antral follicles based on their A4 environment; however, there are relatively few (270 total) transcripts that were significantly different between the High A4 GC and Control GC microarray (Fig. 4, Data in Brief, Snider et al., XXXXXXXX). The fact that most of the transcriptome is similar between High A4 and Control GCs is not surprising, as the samples are from the same cell type and within follicles of the same stage. Interestingly, one of the transcripts with the greatest increase (6.6 fold) in the High A4 GCs is *CYP17A1* (Table 3). This, combined with the fact that the expression of *CYP19A1* was unchanged, corresponds well with the previously identified increases in androgen concentrations within antral follicles (Summers et al., 2014). This suggests that production of A4 by the GCs themselves could be contributing to the local A4 excess.

4.2. Proliferation of GCs are inhibited by a high-androstenedione microenvironment

Additional predicted functional consequences of a high-androgen microenvironment were identified based on analysis of the microarray data with IPA predictive algorithms. The largest category (23%) of downregulated gene functions and the majority of the predicted inhibited cell behaviors were related to mitosis, the cell cycle, and cell proliferation (Fig. 5B, Table 5). Many of the downregulated gene functions that were not directly identified as controlling proliferation can also be related to various aspects of the cell cycle such as DNA replication and repair, chromatin structure, and cytoskeletal dynamics (Fig. 5B). The upregulated gene functions were dominated by miRNA (26%), signaling (17%), and immune function (14%) (Figs. 5A and 7).

Typically, GCs continue to proliferate until terminal differentiation following the peri-ovulatory LH surge. The effects of A4 on GC proliferation have not been previously investigated, but proliferation of GCs *in vivo* can be inhibited by exogenous dihydrotestosterone (DHT) in rats (Kayampilly and Menon, 2012; Pradeep et al., 2002). Thus, to establish whether the A4 concentrations were sufficient to cause inhibited proliferation, in vitro granulosa cell culture experiments were performed. Treatment with A4 resulted in inhibition of granulosa cell proliferation at the greatest A4 dose which was similar to that found in High A4 follicular fluid (Fig. 6) when compared to the untreated control group. The three concentrations of A4 used in this study represent the average A4 concentration in Control follicles (1 nM), an intermediate concentration (100 nM), and the highest A4 concentrations in follicles of the High A4 population (1 μM). These results demonstrate that increased A4 is sufficient to cause the reduction in cell proliferation that was predicted by changes in mRNA abundance. It may be that inhibition of GC proliferation limits the number of cells in the GC population as a whole and thus, reduces the conversion of theca-derived A4 to E2 (Summers et al., 2014). Another potential reason for GC inhibition is due to the increased A4 environment. A study by Billig et al. demonstrated granulosa cells exposed to increased levels of androgens undergo autophagy leading to apoptosis due to increased DNA fragmentation (Billig et al., 1993). Therefore, suppressed GC proliferation may further contribute to the local A4 accumulation and increased GC autophagy and apoptosis.

4.3. Potential regulators inhibiting GC proliferation

Besides A4 exposure itself, regulatory mechanisms resulting in decreased proliferation were investigated. The IPA predictive software was able to determine many signaling molecules, drugs, and signaling mediators like kinases and phosphatases that could potentially cause changes in transcript abundance (Data in Brief, Snider et al., XXXXXXXX). The software can also determine likely upstream regulators and/or inhibitors in the transcripts of interest. However, some of the predicted molecules are unlikely to be present in the follicle, and others do not correspond to known follicular conditions. For example, estrogen is a predicted inhibited upstream regulator, but the estrogen concentrations of the follicles were not lower in the High A4 cows and the expression of the estrogen receptor mRNA is unchanged. There also might be a problem in binding affinity of the estrogen receptor or increased inhibitor production, however, these were not measured and would need to be investigated further. Additionally, neither androgen receptor nor any androgens are predicted upstream regulators as activated by IPA. This may be due to the relative lack of known genetic/molecular interactions for androgens in the IPA database compared to estrogen and other molecules. Nevertheless, the predictions do provide potential avenues of investigation for future assessments of the *in vivo* phenotype.

In addition to the intracellular signaling mediators predicted by the IPA upstream molecules algorithms, miRNA are possible drivers of the inhibited GC proliferation. The ten miRNAs upregulated in the High A4 GCs could be acting on multiple mRNA targets to inhibit cell cycle progression (Data in Brief, Snider et al., XXXXXXXX and Fig. 7). Some of these miRNA are known to inhibit tumor cell proliferation including miR-211 in ovarian epithelial cancer, miR-326 in brain tumors, miR-449B in both ovarian and colon cancer, miR-483 in ovarian and other squamous cell cancers, and miR-584 in various types of cancer (Bertero et al., 2013; Chen, 2013; Kefas et al., 2009; Ma et al., 2011; Ueno et al., 2011; Vriens et al., 2012; Wang et al., 2010; Xia et al., 2015; Zheng et al., 2013). Further investigation is necessary, however, to elucidate the role of these miRNA in a bovine ovarian follicle context.

4.4. High-androstenedione microenvironments may alter cell signaling pathways to compensate for altered steroidogenesis and proliferation

Steroidogenesis and proliferation in GCs are believed to require CTNNB1, a transcriptional co-activator within the WNT signaling pathway, which is inactivated and degraded upon phosphorylation (Castanon et al., 2012; Hernandez Gifford et al., 2009; Liu et al., 2009). Prior studies have documented a greater abundance of total CTNNB1 in cultured bovine GCs following treatment with FSH, and knockdown of CTNNB1 has been shown to inhibit the proliferation of cultured mouse GCs (Castanon et al., 2012; Gupta, et al., 2014; Wang et al., 2010). In the current study, FSH plus 1 μM A4 treatment inhibited proliferation of cultured GCs, and microarray analysis of High A4 GCs indicated inhibition of the cell cycle. Consequently, we predicted that active CTNNB1 would be less abundant in High A4 GCs compared to Control A4 GCs. However, active CTNNB1 was more abundant in High A4 GCs, suggesting that this increase may be a compensatory mechanism. We suggest this, because expression of *CTNNBIP1* mRNA abundance (possibly via increased AMH concentration) was observed in slaughterhouse granulosa cells treated with FSH and A4 at concentrations seen in our High A4 cow dominant follicle follicular fluid. The enhanced AMH and *CTNNBIP1* may lead to reductions in downstream WNT signaling effects (Park et al., 2017).

In GCs, AMH binds to its receptor AMHR2 to regulate cellular proliferation and follicular progression (Poole et al., 2016). Increased AMH concentration has been demonstrated to decrease aromatase (CYP19A1) activity and inhibit the effects of FSH on follicular progression in rodents and women with PCOS (Durlinger et al., 2001; Sacchi et al., 2015). Along with decreasing the effect of FSH in GCs, AMH can increase the expression of *CTNNBIP1* transcripts. The expression of *CTNNBIP1* can inhibit the action of active CTNNB1 and decrease WNT signaling pathway downstream effects (Tago et al., 2000). Reduction in WNT signaling leads to increased GC arrest and inhibition of follicular progression (Durlinger et al., 2001; Park et al., 2017). The increased concentration of active CTNNB1 in the High A4 GC may represent a compensatory response to reverse inhibition of granulosa cell proliferation since normally active CTNNB1 translocates to the nucleus and binds to other transcriptional regulators such as TCF to increase cellular proliferation (Park et al., 2017) or SF1 (NR5A1) to regulate CYP19A1 (Parakh et al., 2006) and LHCGR expression (Law et al., 2013). CTNNB1 is predicted through the IPA upstream analysis to be inhibited in the High A4 granulosa cells, however we have increased active CTNNB1. Normally this increase would indicate that the cell is actively proliferating through the WNT pathway upon binding of active CTNNB1 and TCF. Elevated CTNNBIP1 can block WNT signal transduction by inhibiting binding of TCF and active CTNNB1. Thus, we are hypothesizing that elevated A4 concentrations are inducing AMH-associated *CTNNBIP1* expression, to block proliferation through WNT-active CTNNB1-TCF mechanisms. The culmination of these events inhibits the WNT pathway and may be a cause of the cell cycle arrest and apoptosis in granulosa cells from the High A4 cows.

4.5. CYP17A1, CYP19A1 expression in bovine ovarian follicles

In GCs, the steroidogenesis pathway prior to ovulation involves the conversion of A4 to estrogen with the enzyme aromatase (CYP19A1).

These cells lack the capability to produce this androgen and require A4 produced by theca cells to synthesize estrogens. The enzyme, CYP17A1, along with HSD3β is required to convert pregnenolone to A4. However, recent studies have found a signaling pathway that causes a silence of CYP17A1 in GCs, leading to increased expression of CYP19A1 and the production of estrogen. FOS, an integral activator protein has been demonstrated to be the key regulator of CYP17A1 expression in both theca and granulosa cells, with increased expression in the granulosa cells and the opposite in theca cells (Beshay et al., 2007; Patel et al., 2009).

Patel et al. demonstrated that suppression of *FOS* expression in the HGL5 human granulosa cell line results in robust increases in *CYP17A1* promoter activity and protein expression (Patel et al., 2009). Other studies with KGN cell lines and porcine GCs also demonstrated similar results (Huang et al., 2016; Ye et al., 2017). A study by Shanker et al., determined increased secretion of androgens in prostatic cancer cells suppresses the expression of *FOS* and *JUN* transcripts, leading to altered androgen-receptor signaling (Shanker et al., 2016). Finally, *FOS* is under expressed in adipose tissue of women diagnosed for PCOS and 3 SNP's within the *FOS* gene were significantly associated with PCOS suggesting that individuals with these SNP's were more susceptible for developing PCOS (Jones et al., 2012).

Microarray analysis of control and High A4 GCs showed a 3-fold down regulation of *FOS* and 2-fold down regulation of *JUN* in High A4 GCs and a 6-fold up-regulation of *CYP17A1*, which supports previous reports of altered expression in GCs (Patel et al., 2009). The increased concentration of A4 in follicular fluid of the High A4 cows might be a potential pathway for A4-mediated downregulation of *FOS* and *JUN*, resulting in upregulation of *CYP17A1*. Together, this provides support that High A4 GCs have an altered signaling pathway leading to a loss of identity of these cells.

4.6. High-androstenedione microenvironments may drive partial luteinization

A comparison between the transcriptomes of the High A4 GCs, Control GCs, LLCs, and SLCs reveals differentially regulated transcripts in High A4 GCs have a luteal-like expression pattern. However, there are also other transcripts that are upregulated in High A4 GCs that appear to be theca-specific (*COL4A1*, *AS3MT*, and *CYP17A1*; Table 7). We used Principal Component Analysis (PCA) to visualize variability and identify similarity of cell types. This analysis showed no clear clustering of the High A4 GCs with either luteal cell type; but, does show a modest shift of the High A4 GCs towards the luteal cells based on PCA 1, which represents ~84% of the variability between cell types (Fig. 9). The fact that some of the Control and High A4 GCs overlap in the PCA graph indicates that either the differential gene expression in the High A4 GCs is not robust enough to completely separate the two GC populations using overall transcriptome data or a larger sample size is necessary to identify clear clustering of High A4 GCs separate from Control GCs.

Further investigation into the High A4 GC identity was performed by cross-referencing the set of genes differentially regulated in the High A4 GCs with published transcriptome data from the follicular (GC and TC) and luteal (LLC and SLC) cells of the ovary (Romereim et al., 2016). It is apparent that much of the GC-specific gene expression is lost in the High A4 GC, but there are also no large increases in the expression of genes enriched in luteal cell. Thus, the data does not directly implicate the adoption of another cell identity. From the published list of transcripts specifically enriched in GCs, the High A4 GCs have 87 GC markers with altered expression in the High A4 GCs (Data in Brief, Snider et al., XXXX). Five transcripts were either highest or lowest fold-change differences in the High A4 GCs compared to all other cell populations, indicating a shift away from all other cell types. The other genes were expressed highest in the Control GCs, and the High A4 GCs lost magnitude of expression bringing their expression levels closer to that of the TCs, LLCs, and SLCs. However, none of the identified LLC or SLC markers (Romereim et al., 2016) had significantly increased expression in the High A4 GCs, and there were only three genes that are TC-enriched genes that were significantly increased in expression in the High A4 GCs (Data in Brief, Snider et al., XXXX). The lack of increased expression in genes that are important cell type identifiers suggests that the High A4 GCs have lost their granulosa cell identity and are neither granulosa cells nor luteal cells. This is further supported by 74 changes in expression of genes in High A4 GCs that shifted expression towards the shared luteal gene profiles, but there were also 17 genes indicating a shift in the opposite direction away from luteal patterns. Most of the genes indicating a High A4 GC shift towards a luteal expression pattern were those involved with mitosis and the cell cycle (with luteal cells being less proliferative than pre-ovulatory GCs). For this reason, the High A4 GCs appear to have lost their cellular function and identity.

Finally, it is possible is that the High A4 GCs are undergoing a change that could lead to a persistent or cystic follicle. Bovine and rodent GCs in persistent follicles or cysts have been shown to have GCs with reduced proliferation (Isobe and Yoshimura, 2007; Salvetti et al., 2009). The mechanisms driving inhibition of proliferation in GCs in both a high androgen follicular environment and in the case of follicular persistence will both benefit from further investigation.

4.7. Conclusions

The consequence of a high A4 microenvironment have been investigated using a unique, naturally occurring bovine model of local androgen excess. A thorough analysis of the transcriptomes of the GCs from Control follicles and High A4 follicles has determined that a small set of differentially represented transcripts has important biological relevance to these cells. The High A4 GCs have the potential to contribute to the A4 accumulation and are very likely experiencing inhibited proliferation. Treatment of GCs with A4 in culture is sufficient to decrease expression of the proliferation marker PCNA, increase AMH production, and increase *CTNNBIP1* expression. The increased expression of *CTNNBIP1* can lead to decreased downstream effects to inhibit active CTNNB1 and the WNT signaling pathway, resulting in cell cycle arrest. Additionally, potential upstream regulators of proliferation including miRNA have been identified. Overall, the consequences of excess androgens for GCs are primarily decreased proliferation and loss of cell identity.

Support

This research was supported by USDA-National Institute of Food and Agriculture 2013-67015-20965 and 2017-67015-26450 to ASC, JRW and JSD, University of Nebraska Foundation-Food for Health Competitive Grants to ASC, JSD, and JRW. United States Department of Agriculture Hatch grant NEB26-202/W3112 Accession #1011127 to ASC, United States Department of Agriculture Hatch–NEB Animal Health (ANHL) Accession #1002234 to ASC and JRW and USDA-NIFA postdoctoral fellowship 2016-67012-24697 to SR, USDA-NIFA postdoctoral fellowship 2019-67012-29624 to AS. JSD is a recipient of a Senior Research Career Scientist award from the Department of Veterans Affairs.

Author contribution statement

Dr. Summers synchronized estrous cycles of cows to enable timed follicle collection. Drs McFee, Cushman and Cupp conducted ovariectomies to obtain ovaries to collect granulosa cells. William Pohlmeier isolated GCs with help from Drs. Wood and Cupp and performed RNA isolation with Dr. Summers. Drs. Romereim, McFee and Snider performed data analysis, qPCR, and cell culture. Drs. Romereim and Snider performed immunostaining, and Dr. Snider performed AMH assays and *CTNNBIP1* ddPCR and Dr. Romereim, Dr. McFee and Scott Kurz performed Western blot analysis. Drs. McFee, Romereim and Snider

performed data analysis and wrote the manuscript with guidance and feedback from Drs. Wood, Davis, and Cupp. Drs. Cupp, Wood, Davis obtained the funding for and determined the experimental design for this paper.

Declaration of competing interest

The U.S. Department of Agriculture (USDA) prohibits discrimination in all its programs and activities on the basis of race, color, national origin, age, disability, and where applicable, sex, marital status, familial status, parental status, religion, sexual orientation, genetic information, political beliefs, reprisal, or because all or part of an individual's income is derived from any public assistance program. (Not all prohibited bases apply to all programs.) Persons with disabilities who require alternative means for communication of program information (Braille, large print, audiotape, etc.) should contact USDA's TARGET Center at (202) 720–2600 (voice and TDD). To file a complaint of discrimination, write to USDA, Director, Office of Civil Rights, 1400 Independence Avenue, S. W., Washington, D.C. 20250–9410, or call (800) 795–3272 (voice) or (202) 720–6382 (TDD). USDA is an equal opportunity provider and employer.

Acknowledgements

The authors would like to acknowledge the assistance of the University of Nebraska Medical Center Genomics Core Facility for performing the microarrays and the University of Nebraska-Lincoln Department of Statistics for their help in incorporating the Principal Component Analysis. The University of Nebraska Medical Center Genomics Core receives partial support from the National Institute for General Medical Science (NIGMS) INBRE - P20GM103427-14 and NIH COBRE - 1P30GM110768-01 grants as well as The Fred & Pamela Buffett Cancer Center Support Grant - P30CA036727. This publication's contents are the sole responsibility of the authors and do not necessarily represent the official views of the NIH or NIGMS.

References

Abedal-Majed, M.A., Cupp, A.S., 2019 July. Livestock animals to study infertility in women. Animal Frontiers 9 (3), 28–33. https://doi.org/10.1093/af/vfz017.

Azziz, R., Carmina, E., Dewailly, D., Diamanti-Kandarakis, E., Escobar-Morreale, H.F., Futterweit, W., Janssen, O.E., Legro, R.S., Norman, R.J., Taylor, A.E., Witchel, S.F., 2009. The Androgen Excess and PCOS Society criteria for the polycystic ovary syndrome: the complete task force report. Fertil. Steril. 91, 456–488. https://doi.org/10.1016/j.fertnstert.2008.06.035.

Azziz, R., Sanchez, L.A., Knochenhauer, E.S., Moran, C., Lazenby, J., Stephens, K.C., Taylor, K., Boots, L.R., 2004. Androgen excess in women: experience with over 1000 consecutive patients. J. Clin. Endocrinol. Metab. 89, 453–462. https://doi.org/10.1210/jc.2003-031122.

Balen, A.H., Conway, G.S., Kaltsas, G., Techatraisak, K., Manning, P.J., West, C., Jacobs, H.S., 1995. Andrology: polycystic ovary syndrome: the spectrum of the disorder in 1741 patients. Hum. Reprod. 10, 2107–2111. https://doi.org/10.1093/oxfordjournals.humrep.a136243.

Bateman, H.L., Patisaul, H.B., 2008. Disrupted female reproductive physiology following neonatal exposure to phytoestrogens or estrogen specific ligands is associated with decreased GnRH activation and kisspeptin fiber density in the hypothalamus. Neurotoxicology 29, 988–997. https://doi.org/10.1016/j.neuro.2008.06.008.

Bertero, T., Bourget-Ponzio, I., Puissant, A., Loubat, A., Mari, B., Meneguzzi, G., Auberger, P., Barbry, P., Ponzio, G., Rezzonico, R., 2013. Tumor suppressor function of miR-483-3p on squamous cell carcinomas due to its pro-apoptotic properties. Cell Cycle 12, 2183–2193. https://doi.org/10.4161/cc.25330.

Beshay, V.E., Havelock, J.C., Sirianni, R., Ye, P., Suzuki, T., Rainey, W.E., Carr, B.R., 2007. The mechanism for protein kinase C inhibition of androgen production and 17α-hydroxylase expression in a theca cell tumor model. J. Clin. Endocrinol. Metab. 92, 4802–4809. https://doi.org/10.1210/jc.2007-1394.

Billig, H., Furuta, I., Hsueh, A.J.W., 1993. Estrogens inhibit and androgens enhance ovarian granulosa cell apoptosis. Endocrinology 133, 2204–2212. https://doi.org/10.1210/endo.133.5.8404672.

Castanon, B.I., Stapp, A.D., Gifford, C.A., Spicer, L.J., Hallford, D.M., Hernandez Gifford, J.A., 2012. Follicle-stimulating hormone regulation of estradiol production: possible involvement of WNT2 and beta-catenin in bovine granulosa cells. J. Anim. Sci. 90, 3789–3797. https://doi.org/10.2527/jas.2011-4696.

Chen, Z., 2013. miR-449b inhibits the proliferation of SW1116 colon cancer stem cells through downregulation of CCND1 and E2F3 expression. Oncol. Rep. https://doi.org/10.3892/or.2013.2465.

Conley, A.J., Bird, I.M., 1997. The role of cytochrome P450 17ot-hydroxylase and 31-hydroxysteroid dehydrogenase in the integration of gonadal and adrenal steroidogenesis via the Δ5 and Δ4 pathways of steroidogenesis in mammals. Biol. Reprod. 56, 789–799. https://doi.org/10.1095/biolreprod56.4.789.

Conley, A.J., Kaminski, M.A., Dubowsky, S.A., Jablonka-Shariff, A., Redmer, D.A., Reynolds, L.P., 1995. Immunohistochemical localization of 3 beta-hydroxysteroid dehydrogenase and P450 17 alpha-hydroxylase during follicular and luteal development in pigs, sheep, and cows. Biol. Reprod. 52, 1081–1094. https://doi.org/10.1095/biolreprod52.5.1081.

Dierich, A., Sairam, M.R., Monaco, L., Fimia, G.M., Gansmuller, A., LeMeur, M., Sassone-Corsi, P., 1998. Impairing follicle-stimulating hormone (FSH) signaling in vivo: targeted disruption of the FSH receptor leads to aberrant gametogenesis and hormonal imbalance. Proc. Natl. Acad. Sci. Unit. States Am. 95, 13612–13617. https://doi.org/10.1073/pnas.95.23.13612.

Durlinger, A.L.L., Gruijters, M.J.G., Kramer, P., Karels, B., Kumar, T.R., Matzuk, M.M., Rose, U.M., de Jong, F.H., Uilenbroek, J.T.J., Grootegoed, J.A., Themmen, A.P.N., 2001. Anit-müllerian hormone attenuates the effects of FSH on follicle development in the mouse ovary. Endocrinolgoy 142, 4891–4899. https://doi.org/10.1210/endo.142.11.8486.

Echternkamp, S.E., Roberts, A.J., Lunstra, D.D., Wise, T., Spicer, L.J., 2004. Ovarian follicular development in cattle selected for twin ovulations and births. J. Anim. Sci. 82, 459–471. https://doi.org/10.2527/2004.822459x.

Guilbault, L.A., Roy, G.L., Grasso, F., Matton, P., 1988. Influence of pregnancy on the onset of oestrus and luteal function after prostaglandin-induced luteolysis in cattle. J. Reprod. Fertil. 84, 461–468. https://doi.org/10.1530/jrf.0.0840461.

Hambridge, H.L., Mumford, S.L., Mattison, D.R., Ye, A., Pollack, A.Z., Bloom, M.S., Mendola, P., Lynch, K.L., Wactawski-Wende, J., Schisterman, E.F., 2013. The influence of sporadic anovulation on hormone levels in ovulatory cycles. Hum. Reprod. 28, 1687–1694. https://doi.org/10.1093/humrep/det090.

Hampton, J.H., Manikkam, M., Lubahn, D.B., Smith, M.F., Garverick, H.A., 2004. Androgen receptor mRNA expression in the bovine ovary. Domest. Anim. Endocrinol. 27, 81–88. https://doi.org/10.1016/j.domaniend.2004.01.005.

Hayek, S., Bitar, L., Hamdar, L.H., Mirza, F.G., Daoud, G., 2016. Poly cystic ovarian syndrome: an updated overview. Front. Physiol. https://doi.org/10.3389/fphys.2016.00124.

Hernandez Gifford, J.A., Hunzicker-Dunn, M.E., Nilson, J.H., 2009. Conditional deletion of beta-catenin mediated by Amhr2cre in mice causes female infertility. Biol. Reprod. 80, 1282–1292. https://doi.org/10.1095/biolreprod.108.072280.

Isobe, N., Yoshimura, Y., 2007. Deficient proliferation and apoptosis in the granulosa and theca interna cells of the bovine cystic follicle. J. Reprod. Dev. 53, 1119–1124. https://doi.org/10.1262/jrd.19041.

Jones, M.R., Chazenbalk, G., Xu, N., Chua, A.K., Eigler, T., Mengesha, E., Chen, Y.H., Lee, J.M., Pall, M., Li, X., Chen, Y.D.I., Taylor, K.D., Mathur, R., Krauss, R.M., Rotter, J.I., Legro, R.S., Azziz, R., Goodarzi, M.O., 2012. Steroidogenic regulatory factor FOS is underexpressed in polycystic ovary syndrome (PCOS) adipose tissue and genetically associated with PCOS susceptibility. J. Clin. Endocrinol. Metab. 97, E1750. https://doi.org/10.1210/jc.2011-2153.

Kayampilly, P.P., Menon, K.M.J., 2012. AMPK activation by dihydrotestosterone reduces FSH-stimulated cell proliferation in rat granulosa cells by inhibiting ERK signaling pathway. Endocrinology 153, 2831–2838. https://doi.org/10.1210/en.2011-1967.

Kefas, B., Comeau, L., Floyd, D.H., Seleverstov, O., Godlewski, J., Schmittgen, T., Jiang, J., DiPierro, C.G., Li, Y., Chiocca, E.A., Lee, J., Fine, H., Abounader, R., Lawler, S., Purow, B., 2009. The neuronal MicroRNA miR-326 acts in a feedback loop with notch and has therapeutic potential against brain tumors. J. Neurosci. 29, 15161–15168. https://doi.org/10.1523/JNEUROSCI.4966-09.2009.

Law, N.C., Weck, J., Kyriss, B., Nilson, J.H., Hunzicker-Dunn, M., 2013. Lhcgr expression in granulosa cells: roles for PKA-phosphorylated β-catenin, TCF3, and FOXO1. Mol. Endocrinol. 27, 1295–1310. https://doi.org/10.1210/me.2013-1025.

Liu, Z., Rudd, M.D., Hernandez-Gonzalez, I., Gonzalez-Robayna, I., Fan, H.Y., Zeleznik, A.J., Richards, J.S., 2009. FSH and FOXO1 regulate genes in the sterol/steroid and lipid biosynthetic pathways in granulosa cells. Mol. Endocrinol. 23, 649–661. https://doi.org/10.1210/me.2008-0412.

Luo, W., Wiltbank, M.C., 2006. Distinct regulation by steroids of messenger RNAs for FSHR and CYP19A1 in bovine granulosa cells. Biol. Reprod. 75, 217–225. https://doi.org/10.1095/biolreprod.105.047407.

Lynch, K.E., Mumford, S.L., Schliep, K.C., Whitcomb, B.W., Zarek, S.M., Pollack, A.Z., Bertone-Johnson, E.R., Danaher, M., Wactawski-Wende, J., Gaskins, A.J., Schisterman, E.F., 2014. Assessment of anovulation in eumenorrheic women: comparison of ovulation detection algorithms. Fertil. Steril. 102 https://doi.org/10.1016/j.fertnstert.2014.04.035, 511–518.e2.

Ma, L. ping, Li, N., He, X. jun, Zhang, Q., 2011. [miR-449b and miR-34c on inducing down-regulation of cell cycle-related proteins and cycle arrests in SKOV3-ipl cell, an ovarian cancer cell line]. Beijing Da Xue Xue Bao 43, 129–133.

Mason, H.D., Willis, D.S., Beard, R.W., Winston, R.M., Margara, R., Franks, S., 1994. Estradiol production by granulosa cells of normal and polycystic ovaries: relationship to menstrual cycle history and concentrations of gonadotropins and sex steroids in follicular fluid. J. Clin. Endocrinol. Metab. 79, 1355–1360. https://doi.org/10.1210/jcem.79.5.7962330.

Merke, D.P., Bornstein, S.R., 2005. Congenital adrenal hyperplasia. Lancet 365, 2125–2136. https://doi.org/10.1016/S0140-6736(05)66736-0.

Nkuuhe, J.R., Manns, J.G., 1985. Relationship between time of prostaglandin injection and ovulation in beef cattle. Can. J. Anim. Sci. 65, 405–409. https://doi.org/10.4141/cjas85-047.

Padwal, 2020. Poly cystic ovarian syndrome (PCOS): a review. J. Sci. 3, 12–19.
Parakh, T.N., Hernandez, J.A., Grammer, J.C., Weck, J., Hunizker-Dunn, M., Zeleznik, A. J., Nilson, J.H., 2006. Follicle-stimulating hormone/cAMP regulation of aromatase gene expression requires beta-catenin. Proc. Natl. Acad. Sci. Unit. States Am. 103, 12435–12440. https://doi.org/10.1073/pnas.0603006103.
Park, S.H., Chung, Y.J., Song, J.Y., Kim, S.I., Pépin, D., MacLauglin, D.T., Donahoe, P.K., Kim, J.H., 2017. Müllerian inhibing substance inhibits an ovarian cancer cell line via β-catenin interating protein dergulation for the Wnt signal pathway. Internation Journal of Oncology 50, 1022–1028. https://doi.org/10.3892/ijo.2017.3874.
Patel, S.S., Beshay, V.E., Escobar, J.C., Suzuki, T., Carr, B.R., 2009. Molecular mechanism for repression of 17α-hydroxylase expression and androstenedione production in granulosa cells. J. Clin. Endocrinol. Metab. 94, 5163–5168. https://doi.org/10.1210/jc.2009-1341.
Poole, D.H., Ocón-Grove, O.M., Johnson, A.L. Anti-Müllerian hormone (AMH) receptor type II expression and AMH activity in bovine granulosa cells. Theriogenology 86, 1353-1360. doi: 10.1016/j.theriogenology.2016.04.078.
Pradeep, P.K., Li, X., Peegel, H., Menon, K.M.J., 2002. Dihydrotestosterone inhibits granulosa cell proliferation by decreasing the cyclin D2 mRNA expression and cell cycle arrest at G1 phase. Endocrinology 143, 2930–2935. https://doi.org/10.1210/endo.143.8.8961.
Romereim, S.M., Summers, A.F., Pohlmeier, W.E., Zhang, P., Hou, X., Talbott, H.A., Cushman, R.A., Wood, J.R., Davis, J.S., Cupp, A.S., 2016. Gene expression profiling of bovine ovarian follicular and luteal cells provides insight into cellular identities and functions. Mol. Cell. Endocrinol. 439, 379–394. https://doi.org/10.1016/j.mce.2016.09.029.
Rosenfield, R.L., Ehrmann, D.A., 2016. The Pathogenesis of Polycystic Ovary Syndrome (PCOS): the hypothesis of PCOS as functional ovarian hyperandrogenism revisited. Endocr. Rev. https://doi.org/10.1210/er.2015-1104.
Salvetti, N.R., Panzani, C.G., Gimeno, E.J., Neme, L.G., Alfaro, N.S., Ortega, H.H., 2009. An imbalance between apoptosis and proliferation contributes to follicular persistence in polycystic ovaries in rats. Reprod. Biol. Endocrinol. 7, 68. https://doi.org/10.1186/1477-7827-7-68.
Sacchi, S., D'Ippolito, G., Sena, P., Marsella, T., Tagliasacchi, D., Maggi, E., Argento, C., Tirelli, A., Giulini, S., La Marca, A., 2016. The anti-Müllerian hormone (AMH) acts as a gatekeeper of ovarian steroidogenesis inhibiting the granulosa cell response to both FSH and LH. J. Assist. Reprod. Genet. 33, 95–100. https://doi.org/10.1007/s10815-015-0615-y.
Smith, J.D., Mississippi, S.U., 2015. Cystic ovarian follicles. In: Hopper, R.M. (Ed.), Bovine Reproduction. John Wiley and Sons, pp. 449–455. https://doi.org/10.1002/9781118833971.ch51.
Summers, A.F., Pohlmeier, W.E., Sargent, K.M., Cole, B.D., Vinton, R.J., Kurz, S.G., McFee, R.M., Cushman, R. a, Cupp, A.S., Wood, J.R., 2014. Altered theca and cumulus oocyte complex gene expression, follicular arrest and reduced fertility in cows with dominant follicle follicular fluid androgen excess. PloS One 9, e110683. https://doi.org/10.1371/journal.pone.0110683.
Sunderland, S.J., Crowe, M.A., Boland, M.P., Roche, J.F., Ireland, J.J., 1994. Selection, dominance and atresia of follicles during the oestrous cycle of heifers. J. Reprod. Fertil. 101, 547–555. https://doi.org/10.1530/jrf.0.1010547.
Tago, K., Nakamura, T., Nishita, M., Hyodo, J., Nagai, S., Murata, Y., Adachi, S., Ohwada, S., Morishita, Y., Shibuya, H., Akiyama, T., 2000. Inhibiton of Wnt signaling by ICAT, a novel β-catenin-interacting protein. Gene Dev. 14, 1741–1749. https://doi.org/10.1101/gad.14.14.1741.
Ueno, K., Hirata, H., Shahryari, V., Chen, Y., Zaman, M.S., Singh, K., Tabatabai, Z.L., Hinoda, Y., Dahiya, R., 2011. Tumour suppressor microRNA-584 directly targets oncogene Rock-1 and decreases invasion ability in human clear cell renal cell carcinoma. Br. J. Canc. 104, 308–315. https://doi.org/10.1038/sj.bjc.6606028.
Viau, V., 2002. Functional cross-talk between the hypothalamic-pituitary-gonadal and -adrenal axes. J. Neuroendocrinol. 14, 506–513. https://doi.org/10.1046/j.1365-2826.2002.00798.x.
Vriens, M.R., Weng, J., Suh, I., Huynh, N., Guerrero, M.A., Shen, W.T., Duh, Q.-Y., Clark, O.H., Kebebew, E., 2012. MicroRNA expression profiling is a potential diagnostic tool for thyroid cancer. Cancer 118, 3426–3432. https://doi.org/10.1002/cncr.26587.
Wang, X.-Y., Wu, M.-H., Liu, F., Li, Y., Li, N., Li, G.-Y., Shen, S.-R., 2010. Differential miRNA expression and their target genes between NGX6-positive and negative colon cancer cells. Mol. Cell. Biochem. 345, 283–290. https://doi.org/10.1007/s11010-010-0582-7.
Wiltbank, M., Gümen, A., Sartori, R., 2002. Physiological classification of anovulatory conditions in cattle. Theriogenology 57, 21–52. https://doi.org/10.1016/S0093-691X(01)00656-2.
Xia, B., Yang, S., Liu, T., Lou, G., 2015. miR-211 suppresses epithelial ovarian cancer proliferation and cell-cycle progression by targeting Cyclin D1 and CDK6. Mol. Canc. 14, 57. https://doi.org/10.1186/s12943-015-0322-4.
Young, J.M., McNeilly, a S., 2010. Theca: the forgotten cell of the ovarian follicle. Reproduction 140, 489–504. https://doi.org/10.1530/REP-10-0094.
Youngquist, R.S., Garverick, H.A., Keisler, D.H., 1995. Use of umbilical cord clamps for ovariectomy in cows. J. Am. Vet. Med. Assoc. 207, 474–475.
Zhang, K., Zhu, S., Liu, Y., Dong, X., Shi, Z., Zhang, A., Liu, C., Chen, L., Wei, J., Pu, P., Zhang, J., Jiang, T., Han, L., Kang, C., 2015. ICAT inhibits glioblastoma cell proliferation by suppressing Wnt/β-catenin activity. Canc. Lett. 357, 404–411. https://doi.org/10.1016/j.canlet.2014.11.047.
Zheng, H., Zhang, L., Zhao, Y., Yang, D., Song, F., Wen, Y., Hao, Q., Hu, Z., Zhang, W., Chen, K., 2013. Plasma miRNAs as diagnostic and prognostic biomarkers for ovarian cancer. PloS One 8, e77853. https://doi.org/10.1371/journal.pone.0077853.